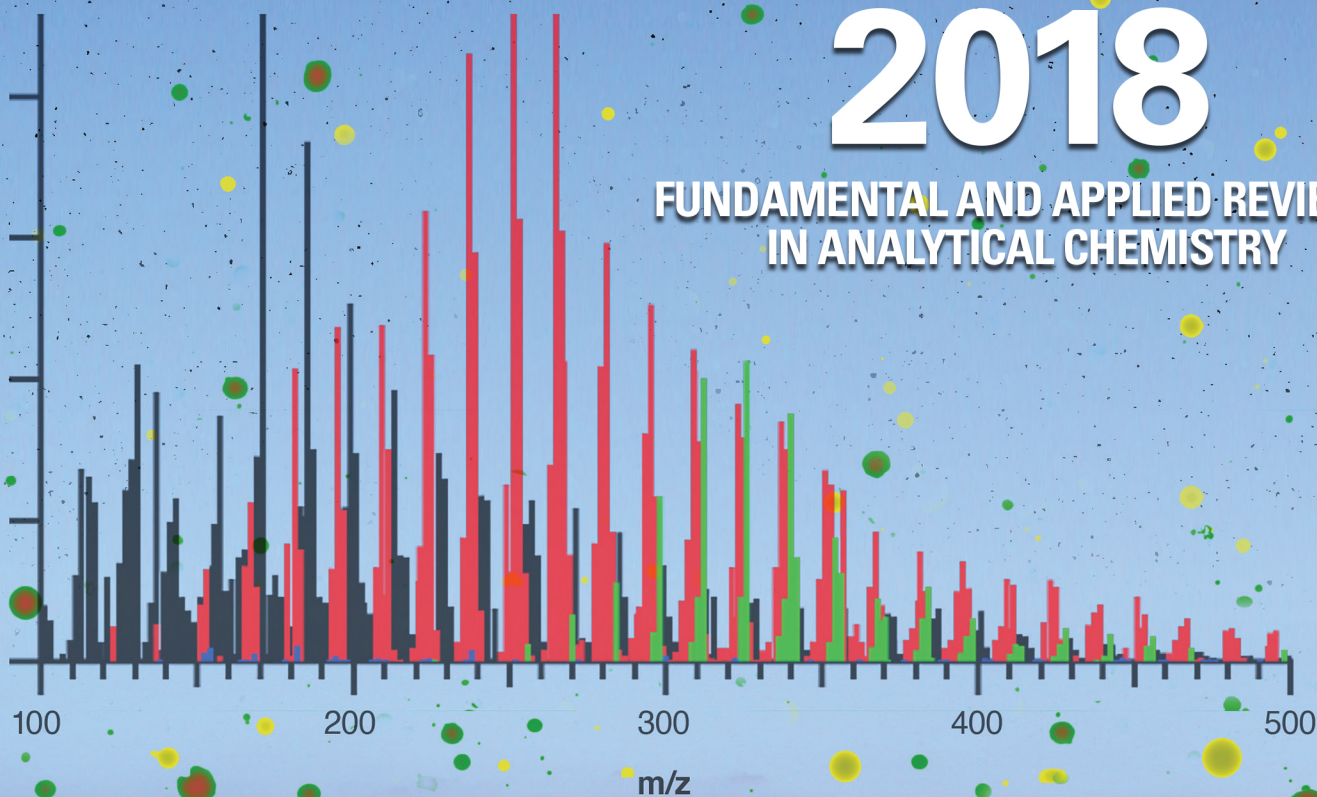


analytical chemistry

January 2, 2018 Volume 90 Number 1

2018

FUNDAMENTAL AND APPLIED REVIEWS
IN ANALYTICAL CHEMISTRY



Mass Spectrometry Analysis in Atmospheric Chemistry

Julia Laskin,^{*,†} Alexander Laskin,[†] and Sergey A. Nizkorodov[‡]

[†]Department of Chemistry, Purdue University, West Lafayette, Indiana 47907, United States

[‡]Department of Chemistry, University of California, Irvine, California 92697, United States

CONTENTS

Advances in Analytical Methods	167
Quantitative Detection of Atmospheric VOCs	167
Ion Mobility for Detection of Gas- and Condensed-Phase Species	168
Novel Ionization Methods for Aerosol Analysis	170
Offline Analysis of Aerosol Samples	171
High-Resolution Mass Spectrometry (HRMS)	171
GC-MS of Collected Particulate Matter	172
High-Performance Liquid Chromatography Mass Spectrometry (HPLC-MS)	172
MS Analysis of Individual Particles	173
Aerosol Mass Spectrometry (AMS)	175
Advances in Laboratory and Field Applications	175
Highly Oxidized Multifunctional Organic Compounds	175
New Particle Formation and Growth	176
Gas-Phase Oxidation of VOC and SOA Formation	177
Aqueous-Phase SOA Chemistry	179
Chemical Aging of Organic Aerosols	180
Volatility and Viscosity of Organic Aerosols	181
Chemistry of Brown Carbon	181
Atmospheric Chemistry at the Air–Water Interface	183
Sea Spray Aerosol	184
Summary and Outlook	184
Author Information	185
Corresponding Author	185
ORCID	185
Notes	185
Biographies	185
Acknowledgments	185
References	186

In the Earth's atmosphere, numerous gas-phase species and airborne particles form a complex mixture called atmospheric aerosol. A variety of natural and anthropogenic primary emission sources along with chemical and photochemical transformations of the emitted compounds in the atmosphere contribute to a large diversity of aerosols, which often contain hundreds of individual components existing in different phases in a dynamic gas-particle exchange.^{1–3} Common examples of atmospheric aerosols include sea-salt spray (SSA), biomass burning organic aerosol (BBOA), mineral dust, soot, biological aerosol, and forest haze. Organic aerosol (OA) is commonly categorized either as a primary organic aerosol (POA) or secondary organic aerosol (SOA) depending on how it is produced. However, this distinction is quickly erased by the chemical and physical aging processes in the atmosphere. In the

aerosol system, concentrations of individual compounds both in the gas- and condensed phases can differ by orders of magnitude. Chemical properties of these species also are remarkably diverse with respect to their molecular weights, structures, volatility, polarity, light absorption, and reactivity.^{4–9}

Furthermore, particles in aerosol mixtures have a distribution of sizes and typically contain several components (internal mixing); mixtures of individual single-component particles (external mixing) are also common. Because of their profound impact on air quality in urban areas, biogeochemical cycling of elements, plant ecology, climate, and human health, atmospheric aerosols have been actively investigated by the scientific community. Assessment and mitigation of aerosols' impact on the environment require detailed experimental speciation of their chemical composition and physical properties, a challenging task that drives the development and applications of novel mass spectrometry (MS) based analytical techniques for aerosol measurements. In this review, we summarize the most recent developments in MS instrumentation and their applications focused on understanding the formation and transformation of OA, one of the most complex and dynamic atmospheric components, with an emphasis on studies published between 2015 and 2017. The review is by no means comprehensive but rather emphasizes the breadth of analytical developments in both online and offline analysis of volatile organic compounds (VOCs) and condensed-phase aerosol components.

In the past 3 decades, MS techniques have been at the forefront of aerosol characterization.^{10,11} MS offers an unmatched potential for both qualitative and quantitative analysis of a broad range of chemical species in OA with high sensitivity and high dynamic range. Inherent versatility in sample introduction, ionization, and mass analysis resulted in numerous innovations in the instrument development and applications. These advances are critical for unraveling the complexity of OA and providing unique information on the aerosol composition and transformations. The broad subject area of MS analysis of atmospheric aerosols, which includes both in situ and offline approaches, has been extensively reviewed.^{10–17} Currently, MS characterization of aerosols is still a rapidly growing area of analytical chemistry that shows no signs of decline. Remarkably, at the time of this manuscript preparation, a search for "Atmospheric Aerosol Mass Spectrometry" on the *Web of Science* resulted in around 2600 manuscripts in peer-reviewed literature with nearly 800 papers published after 2013. This review is organized into two major

Special Issue: Fundamental and Applied Reviews in Analytical Chemistry 2018

Published: October 31, 2017

sections. In the first section, we present new developments in MS instrumentation and methods that advanced various aspects of gas-phase, cluster, and particle measurements. In the second section, we summarize selected applications of MS-based techniques focused on understanding atmospheric chemistry of OA both in field and laboratory studies. Finally, we discuss several promising future directions in this field.

■ ADVANCES IN ANALYTICAL METHODS

In the 2015–2017 time period highlighted in this review, significant efforts have been dedicated to the development of new and improved approaches for the quantitative measurement and structural characterization of aerosol components, identification of light-absorbing molecules in OA, imaging and analysis of individual particles, and understanding reactions at the air–liquid interface. In this section, we initially discuss new methods for the characterization of gaseous aerosol compounds and subsequently present a summary of selected approaches for the analysis of condensed-phase compounds and liquid surfaces.

Quantitative Detection of Atmospheric VOCs. Several groups have developed new approaches for the analysis of ambient volatile organic compounds (VOCs). For example, Perraud et al.¹⁸ used proton transfer reaction-time-of-flight-mass spectrometry (PTR-TOF-MS) and gas chromatography with flame ionization (GC-FID) to accurately measure abundances of ambient organosulfur compounds (OSCs). OSCs produced from various sources are readily removed from the atmosphere through reaction with OH[•] during the day and NO₃[•] at night. Accurate determination of OSC concentrations is critical to understanding new particle formation in the atmosphere. Atmospheric OSC concentrations span several orders of magnitude from low part per trillion by volume (pptv) to hundreds of parts per billion by volume (ppbv). This broad range of concentrations along with reactivity of OSCs both with atmospheric oxidants and surfaces present a challenge for their accurate quantification. PTR-TOF-MS enables real-time quantitative detection of OSCs over a broad range of concentrations with caveats that fragmentation of OSCs following ionization complicates their identification during complex mixture analysis and that isobaric species cannot be distinguished. Complementary offline characterization of OSCs collected into a canister using GC-FID provides accurate concentrations and can distinguish isomers but cannot be used for real-time measurements. Furthermore, reactions of OSCs with the canister walls in GC-FID and sampling lines in PTR-TOF-MS were shown to be an important process with the efficiency strongly dependent on the amount of moisture in the system, which complicates accurate quantification of OSCs in complex mixtures using these techniques.

Barreira et al.¹⁹ developed an approach for the analysis of VOCs in remote locations by combining needle microextraction with a portable gas chromatography-mass spectrometry (GC-MS) instrument. Specifically, air was pumped through a commercially available needle microextraction device packed with sorbent particles using an air sampling interface. The sampling was performed for 100 min at a flow rate of 25 mL/min. The needle was subsequently transferred to the sampling port of a portable GC-MS instrument, and the analysis of the adsorbed VOCs was performed using a 10 s long thermal desorption step. Abundant monoterpenes and aldehydes were quantitatively analyzed over the course of several weeks. An

inverse correlation between particle formation and monoterpene/aldehyde concentrations was reported confirming the important role of biogenic VOCs in the new particle formation.

Dhummakupt et al.²⁰ used paper spray ionization for the analysis of VOCs collected on a glass filter paper. In these experiments, a disposable cartridge containing a glass fiber filter is mounted onto a specially designed 3D-printed holder that enables efficient and reproducible collection of gases onto the substrate. For MS analysis, the substrate is positioned near the MS inlet, a mixture of internal standards and a solvent are dispensed onto the substrate, and the captured VOCs are analyzed by applying a potential to the glass fiber filter. The approach was demonstrated for the analysis of chemical warfare agent simulants aerosolized in an aerosol chamber and for samples collected by mounting paper spray cartridges onto different unmanned vehicles. The reactivity of the collected VOCs with the substrate must be taken into consideration. This study demonstrated that surface derivatization helps alleviate this problem.

Several studies have examined quantification in chemical ionization mass spectrometry (CIMS), a technique ideally suited for the sensitive detection of numerous VOCs. In particular, better understanding of the dependence of adduct formation efficiency in CIMS on the structure and composition of analyte compounds along with accurate characterization of the instrument transmission are necessary for quantification of the observed VOCs. For example, Lopez-Hilfiker et al.²¹ have examined factors affecting the sensitivity of CIMS that employs iodide adduct [M + I]⁻ formation. Iodide adduct formation with analyte molecules occurs at the collision limit making it particularly attractive for CIMS applications. However, weakly bound complexes undergo efficient fragmentation in the gas phase and do not contribute to the observed signal. It follows that declustering of analyte-containing ions is undesirable as it affects the sensitivity and quantification of the observed analytes. To better understand the declustering phenomenon, the authors have determined the relative binding energies of iodide to selected analyte molecules, which affect the instrument sensitivity to different VOCs. They found that even under “mild” source conditions, which minimized collision energy, many iodide adducts underwent fragmentation prior to detection. Declustering scans acquired by scanning the potential between the skimmer and the entrance to the quadrupole ion guide were acquired to facilitate quantification. Fast dissociation of complexes containing monocarboxylic acids and diols makes quantification of these classes of compounds using iodide-CIMS challenging. In contrast, larger multifunctional molecules produce stable adducts that are detected with high sensitivity. Both the number of vibrational degrees of freedom in the cluster and higher iodide binding energy may contribute to the increased stability of the iodide clusters with larger multifunctional molecules. It has been demonstrated that declustering scans enable quantification of hundreds of VOCs, for which standards are not readily available.

In a related study, Iyer et al.²² calculated iodide binding energies to atmospherically relevant organic and inorganic compounds. Comparison with the experimental data demonstrated a linear relationship between the calculated binding energies and logarithmic instrument sensitivities measured using a high-resolution TOF-CIMS instrument. The effect of iodide binding energy on the sensitivity was attributed to the increased stability of the cluster and reduced fragmentation during its transfer through the instrument. Additional kinetic

stabilization was observed for larger clusters and rationalized using Rice–Ramsperger–Kassel–Marcus (RRKM) theory. Specifically, slower fragmentation of larger clusters was attributed to the increase in the number of vibrational degrees of freedom. These findings indicate that electronic structure calculations combined with RRKM treatment of cluster fragmentation rate constants provide reliable predictions of the instrumental sensitivities in iodide-CIMS experiments.

Brophy and Farmer²³ have examined clustering of VOCs with acetate anions in acetate-CIMS experiments. In contrast with iodide-CIMS, in which adduct formation is the dominant ionization mechanism, ions observed in acetate-CIMS experiments are produced both via cluster formation and proton abstraction by acetate ion from acidic volatile analytes. Furthermore, analyte anions produced through proton transfer may undergo subsequent clustering reactions. These clustering processes complicate data interpretation. As a result, efficient declustering in a collision cell is necessary for quantification in acetate-CIMS experiments. Another complication originates from the analyte- and RH-dependent variations in the sensitivity in the presence of water vapor, which makes it difficult to perform nontargeted quantitative analysis using acetate-CIMS.

Similarly, variations in the transmission of the H_3O^+ reagent ions as a function of relative humidity (RH) and instrument parameters have been identified as the most significant challenge for quantitative measurements in H_3O^+ -CIMS experiments.²⁴ In that study, Yuan et al. developed an aircraft-deployable high-resolution time-of-flight instrument for the detection of atmospheric VOCs using chemical ionization with H_3O^+ as a reagent (H_3O^+ TOF-CIMS). The instrument is equipped with a drift tube followed by two quadrupole ion guides and an orthogonal TOF. The instrument enables rapid online measurement of common atmospheric VOCs with high sensitivity and detection limits in the range of 20–500 pptv for a 1 s integration time. The mass resolving power ($m/\Delta m$) of ~ 6000 and mass accuracy of 5–10 ppm enable the separation and identification of isobaric peaks. The instrument performance was validated using independent GC-MS measurements of air samples.

High-resolution TOF-CIMS also has been coupled to a FIGAERO system (Filter Inlet for Gases and AEROSols), which uses temperature programmed desorption to separate organic compounds based on their volatility.²⁵ In that study, acetate-CIMS was employed to characterize acidic compounds present in monoterpene-SOA. It was found that a majority of α -pinene SOA compounds have very low volatility and contain more than ten carbon and four oxygen atoms. A substantial fraction of these compounds have been attributed to oligomeric species that undergo fragmentation during thermal desorption.

Several other CIMS reagents have been evaluated. For example, Simon et al.²⁶ have demonstrated the utility of nitrate-CIMS for the detection of atmospheric amines at subpptv levels. In addition to amines, nitrate-CIMS provides information on the concentration of sulfuric acid and some low-volatility organic compounds, which collectively contribute to the new particle formation in the atmosphere. The approach was implemented on a chemical ionization atmospheric pressure interface time-of-flight mass spectrometer (CI-API-TOF-MS) attached to the Cosmics Leaving Outdoor Droplets (CLOUD) chamber. It has been demonstrated that dimethylamine generates clusters with $\text{NO}_3^-(\text{HNO}_3)_n$ ($n = 1-3$). The results obtained using nitrate-CIMS were in good agreement

with an independent measurement of amine concentrations using ion chromatography.

Kim et al.²⁷ used benzene cations as CIMS reagents for the sensitive detection of dimethyl sulfide, isoprene, α -pinene, and several sesquiterpenes with minimal fragmentation. Field observations in the remote marine boundary layer along with laboratory measurements were used to evaluate the analytical performance and provide insights on the mechanisms of cluster formation in benzene-CIMS. VOCs were detected both as molecular cations ($\text{M}^{+\bullet}$) and as benzene adducts ($\text{M}-(\text{C}_6\text{H}_6)^{+\bullet}$). Similar to other reagent CIMS, the sensitivity of benzene-CIMS is strongly affected by the presence of water vapors. Good correlation between dimethyl sulfide concentrations obtained using benzene-CIMS and atmospheric pressure MS measurements indicate the validity of this approach for quantitative measurements when careful attention is paid to the experimental parameters.

Ion Mobility for Detection of Gas- and Condensed-Phase Species. Several recent studies have focused on the characterization of the structures and reactivity of atmospherically relevant molecules and clusters based on their drift times in mobility cells. For example, Oberreit et al.²⁸ have developed an approach for studying heterogeneous uptake of gas phase molecules onto cluster ions using a combination of differential mobility analysis and mass spectrometry (DMA-MS). They demonstrated sensitive detection of vapor molecule uptake events over a broad range of partial pressures up to saturation by separating ions by both the mobility and mass-to-charge ratio. For example, they observed uptake of 4 to 40 water molecules onto small metal iodide clusters. The extent of water uptake was found to be dependent on the cluster size and structure. The experimental results were compared with predictions of two models: a Langmuir adsorption and Kelvin–Thomson–Raoult (KTR) model. The comparison demonstrated that the KTR model, which assumes the presence of a bulk liquid layer on the surface of the cluster, does not reproduce the experimental data. In contrast, the Langmuir adsorption model adequately describes water uptake by small metal iodide clusters. Similarly, uptake of organic molecules (1-butanol, ethanol, methyl ethyl ketone, and toluene) by both positively and negatively charged sodium chloride cluster ions is consistent with a site-specific, Langmuir-type adsorption of individual vapor molecules onto the cluster.²⁹ In this study, Li and Hogan demonstrated that uptake of vapor molecules is affected both by the structure of the organic molecule and cluster charge polarity but rather independent of the cluster size. These observations were rationalized assuming that electrostatic interactions determined by the electronic structure of individual cluster ions and the properties of the neutral molecule are critical to the initial stages of vapor molecule uptake by clusters.

In a follow up study, Thomas et al.³⁰ used DMA-MS to examine structures of bare and hydrated dimethylamine-sulfuric acid cluster cations of interest to new particle formation. Electrospray ionization (ESI) produced a distribution of $[\text{H}((\text{CH}_3)_2\text{NH})_x(\text{H}_2\text{SO}_4)_{x-1}]^+$ cluster ions, which could be tuned by varying the RH. Substantial fragmentation of the cluster ions makes it difficult to determine their mobility. Cluster hydration at higher RH was shown to produce more stable species. This observation was attributed to the cooling of cluster ions resulting from multiple losses of water molecules in the instrument inlet. The discrepancy between the experimental collision cross sections and the values predicted using the

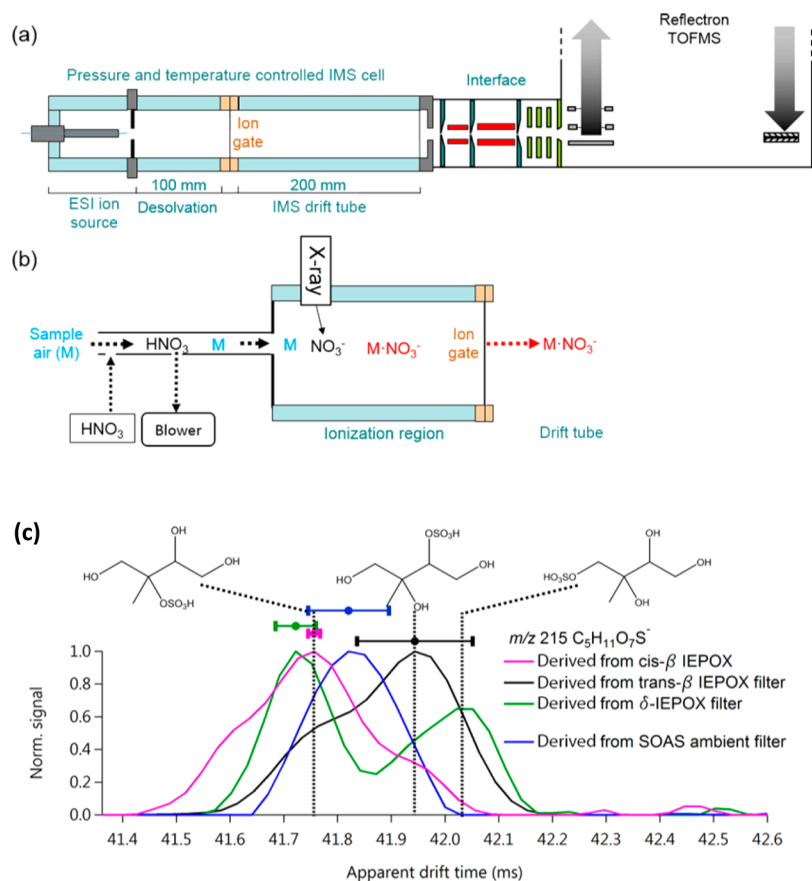


Figure 1. Schematic diagram of the IMS-TOF-MS (a). The instrument can be used with different ionization sources, including the ESI source shown in part a and the custom-built nitrate-ion chemical ionization source (NO_3^- -CI) attached to the front end of the desolvation region shown in part b. (c) Ion mobility spectra of hydroxy sulfate ester $\text{C}_5\text{H}_{11}\text{O}_7\text{S}^-$ in four different aerosol filter samples. Dashed vertical lines indicate the three different IMS peaks/isomers observed in different combinations in each sample. All spectra have been normalized to facilitate qualitative comparison. The bars on the top denote the uncertainty in the drift time dimension for each peak. Reproduced with modifications from Krechmer, J. E.; Groessl, M.; Zhang, X.; Junninen, H.; Massoli, P.; Lambe, A. T.; Kimmel, J. R.; Cubison, M. J.; Graf, S.; Lin, Y. H.; Budisulistiorini, S. H.; Zhang, H. F.; Surratt, J. D.; Knochenmuss, R.; Jayne, J. T.; Worsnop, D. R.; Jimenez, J. L.; Canagaratna, M. R., *Atmospheric Meas. Tech.* **2016**, *9*, 3245–3262 (ref 31), licensed under a Creative Commons Attribution 3.0 Generic License.

Stokes–Millikan equation indicated the importance of understanding the dynamics of cluster-neutral collisions for accurate structural characterization of cluster ions based on their collision cross sections. The authors suggested that fragmentation in the MS inlet must be taken into account when signal intensities observed experimentally are used to quantify absolute or relative cluster concentrations.

Ion mobility spectrometry-mass spectrometry (IMS-MS) has evolved into a powerful tool for the characterization of the structures and molecular formulas of organic species both in aerosol and gas phase. For example, in a study by Krechmer et al.³¹ the online characterization of gas phase species was achieved by coupling a chemical ionization (CI) source with IMS-MS on a TOFWERK instrument (Figure 1a,b). Meanwhile, organic molecules in the aerosol phase were characterized offline using ESI-IMS-MS. Ions produced by ESI are bunched using an ion gate and separated in a drift tube under precisely controlled temperature and pressure. The ability to separate isomeric species was demonstrated using $\text{C}_5\text{H}_{11}\text{O}_7\text{S}^-$ ion (Figure 1c) corresponding to a hydroxy sulfate ester produced via reactions of isoprene epoxydiols (IEPOX) in sulfuric acid seed particles. Arrival time distributions obtained for this ion along with assigned structures of isomeric species are shown in Figure 1c. Three isomers of $\text{C}_5\text{H}_{11}\text{O}_7\text{S}^-$ observed

in IMS-MS experiments are consistent with the known formation mechanisms of this compound, and the relative abundance of these isomers is different for different precursors. Analysis of samples from both laboratory experiments and field Southern Oxidant and Aerosol Study (SOAS) demonstrated the ability of IMS-MS to separate numerous water-soluble organic carbon (WSOC) species that cannot be readily separated using liquid chromatography.

In a related study, Zhang et al.³² used IMS-MS to separate organic molecules in aerosol samples based on their collision cross section. Aerosol samples were dissolved in a solvent containing methanol, water, and formic acid (70:29:1 v/v/v) and ionized using ESI. IMS was used to separate different classes of compounds containing amine, carbonyl, carboxyl, alcohol, ester, and organic sulfate functional groups. For different classes of compounds, experimentally measured collision cross sections showed a linear increase with m/z with a slope unique to each class. This enables separation of different species based on their m/z and collision cross section. In addition, this study demonstrated that IMS-MS provides a convenient way to explore reactions of organic compounds in aerosol samples. To make the method even more versatile, collision-induced dissociation may be used to examine structures for different molecules in complex samples.

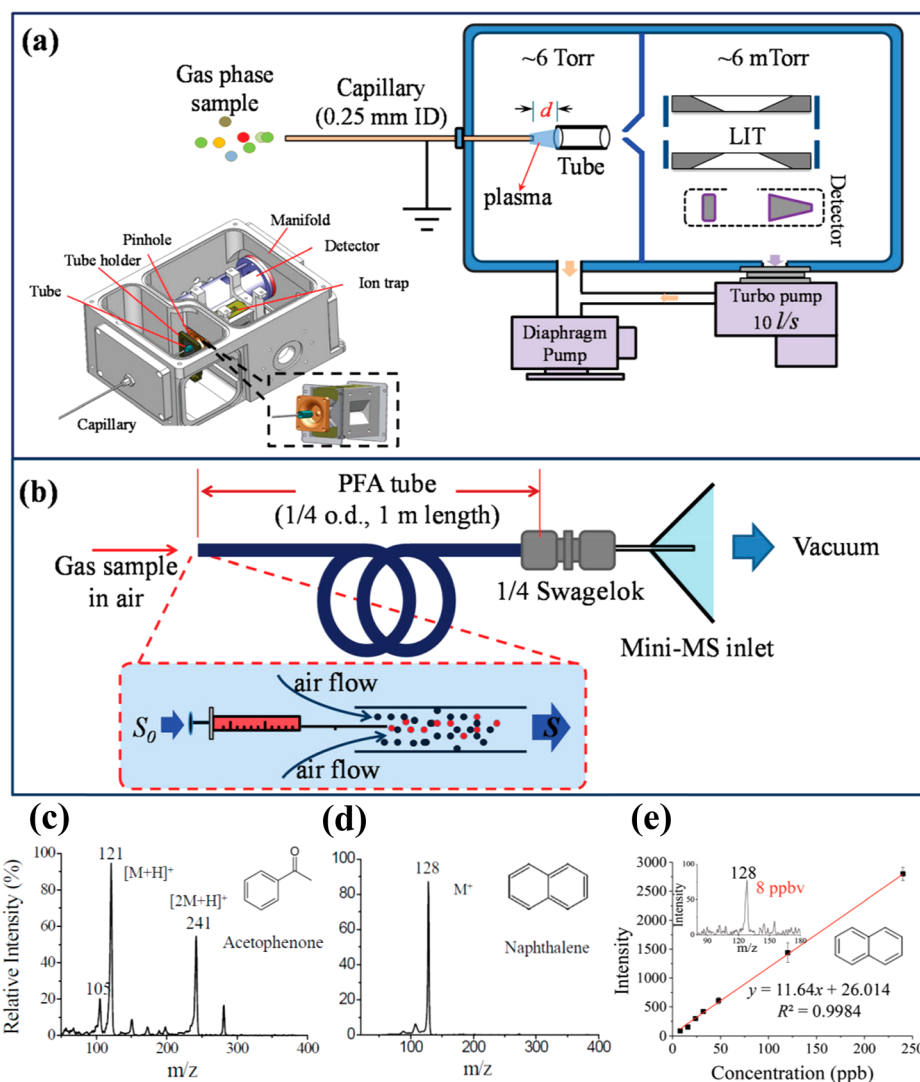


Figure 2. (a) Schematic depiction of the miniature mass spectrometer with an in-vacuum plasma ionization source placed in the first vacuum chamber (~ 6 Torr). (b) Schematic of the apparatus for quantification analysis of gaseous samples. (c,d) Mass spectra of acetophenone (m/z 121) and naphthalene (m/z 128) showing different modes of ionization in the plasma source. (e) Linear range of quantitation curve for naphthalene (m/z 128) with a LOD of 8 ppbv. Reproduced with modifications from Zhai, Y. B.; Jiang, T.; Huang, G. Y.; Wei, Y. Z.; Xu, W., *Analyst* **2016**, *141*, 5404–5411 (ref 35), with permission of The Royal Society of Chemistry.

Novel Ionization Methods for Aerosol Analysis. Horan et al.³³ introduced droplet assisted inlet ionization (DAII) as a method for the online characterization of airborne particles with minimal fragmentation. In this method, the particles are first converted into aqueous droplets and concentrated into an air flow using a custom-designed nanoaerosol sampler.³³ The air flow containing droplets is directed into a heated mass spectrometer inlet, in which rapid evaporation of the droplets produces charged analyte molecules through a process described in detail by Trimpin et al.³⁴ Although the mechanistic details of inlet ionization are still not fully understood, the process results in gentle ionization of analyte molecules. DAII was shown to produce high-quality mass spectra of test aerosols of 10–200 nm in diameter with a temporal resolution of ~ 1 s. The ionization efficiency is strongly dependent on the heated inlet temperature with the optimal value achieved at 850 °C. Aerosol mass concentrations examined in that study were in the range of 10 ng/m³ to 1000 $\mu\text{g}/\text{m}^3$.

Zhai et al.³⁵ reported the development of an in-vacuum plasma ionization source for a miniature mass spectrometer

shown in Figure 2. In addition, an aerodynamic-assisted inlet for VOCs has been installed on this instrument. Collectively, these new capabilities resulted in a dramatic improvement in sensitivity, which was shown to be in tens of ppbv levels for this instrument. Forbes and Staymates introduced a different approach that enables remote sampling and ionization of both VOCs and aerosols.³⁶ In this approach, Venturi-assisted entrainment is coupled with corona discharge ionization in front of a mass spectrometer inlet. This approach increases the collection efficiency of VOCs and particles in ambient air by at least an order of magnitude. Furthermore, efficient transport of analyte molecules enables remote sampling from more than 2.5 m distance from the source.

A commercial direct analysis in real time (DART) source was used for the online analysis of organic aerosol (OA) produced by reactions of submicrometer particles containing dicarboxylic acids with gaseous amines.³⁷ Ionization of analyte molecules in DART is caused by charge exchange reactions with small ions produced through interactions of ambient air with metastable helium atoms generated by a corona discharge. It has been

demonstrated that DART probes the outer surface layer (~ 30 nm thick) of the particles and that particles containing odd-carbon diacids are more reactive than their counterparts containing even-carbon chain species. In a follow-up study from the same group, Kumbhani et al.³⁸ cautioned that ambient ionization methods, including DART, extractive electrospray ionization (EESI), and ionization by piezoelectric direct discharge plasma may suffer from severe contamination resulting from routine cleaning activities in the laboratory. Furthermore, they suggested that the usual practice of subtracting a background air spectrum may not work well in the presence of ionizable organic contaminants in the air.

Flowing atmospheric pressure afterglow (FAPA) has been used for the identification of acidic compounds in limonene-SOA collected on filters.³⁹ In FAPA-MS, excited helium atoms and excimers produced in the flowing afterglow interact with molecules in air to generate ions that subsequently undergo charge exchange reactions with analyte molecules desorbed from substrates. This process generates $[M + H]^+$ and $[M - H]^-$ analyte species with little or no fragmentation. In addition, abundant adducts with O^+ , NO^+ , O_2^+ , NO_2^+ , and NH_4^+ and minor peaks corresponding to fragment ions were observed for single-component standard analytes in positive mode. Meanwhile, negative-mode spectra contained NO_3^- and Cl^- adducts along with abundant deprotonated analyte molecules. It was also reported that oxidation of analyte molecules may occur in plasma, which complicates the interpretation of FAPA-MS spectra. In contrast, only $[M + NO_3]^-$ adducts were observed in negative mode spectra of limonene-SOA. The absence of $[M - H]^-$ species known to dominate FAPA-MS spectra of single-component analytes was attributed to matrix effects. Although the initial results are promising, additional studies are required to obtain a better understanding of complex mixture analysis in FAPA ionization.

Analysis of the chemical composition of nanoparticles is challenging because of the tiny amount of material these particles contain. This challenge was overcome more than 10 years ago by collecting nanoparticles using electrostatic precipitation onto a sharp metal tip and then thermally desorbing them for analysis by CIMS.⁴⁰ A related approach was developed recently, in which a tungsten tip coated with collected particles is used as an ESI emitter.⁴¹ This approach enables soft ionization of OA components for subsequent analysis using mass spectrometry. Electrostatic precipitation is performed by passing mostly neutral ambient particles through a corona discharge ionization chamber and depositing charged particles onto the collection tip. This approach efficiently discriminates against volatile components and neutral particles. Highly efficient detection of particles with mass concentrations down to $10^{-2} \mu\text{g}/\text{m}^3$ has been demonstrated. However, it was shown that analyte solubility in the ESI solvent and the stability of the Taylor cone may affect quantification and sensitivity toward different analytes. The compact size and ease of use of this instrument make it a promising system for field implementation.

Thomas et al.⁴² introduced two new methods for the analysis of liquid surfaces: bursting bubble ionization (BBI) and interfacial sampling with an acoustic transducer (ISAT) ionization approaches. These techniques are schematically shown in Figure 3. In the first approach, sampling from liquid surfaces is achieved through bubble bursting that generates small charged droplets containing analyte molecules from the interfacial region. Subsequent droplet desolvation in a mass

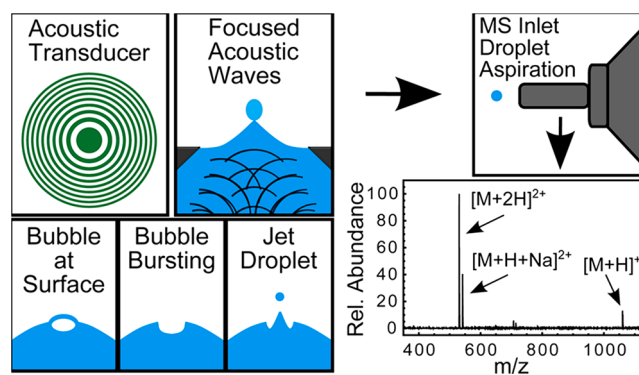


Figure 3. Schematic representation of bursting bubble ionization (BBI) and interfacial sampling with an acoustic transducer (ISAT), the MS inlet, and a typical mass spectrum obtained for a $50 \mu\text{M}$ solution of bradykinin. Reproduced from Thomas, D. A.; Wang, L. T.; Goh, B.; Kim, E. S.; Beauchamp, J. L., *Anal. Chem.* **2015**, *87*, 3336–3344 (ref 42). Copyright 2015 American Chemical Society.

spectrometer inlet generates ions of intact analyte molecules. Alternatively, liquid surfaces may be interrogated using an acoustic transducer that generates regions of constructive interference on the liquid surface, from which droplets are ejected. Acoustic droplet generation produces droplets with diameters in a range of $10\text{--}100 \mu\text{m}$ with volumes down to 0.5 pL . Droplet size is limited by the acoustic wave frequency in water and can be adjusted by selecting an appropriate harmonics of the resonant frequency. Larger droplets ($\sim 250 \mu\text{m}$ in diameter) are produced using bursting bubble mode. The capabilities of these techniques have been characterized by examining the oxidation of oleic acid by ozone that has been extensively studied using different analytical methods. Characteristic products of oleic acid oxidation were detected as a function of reaction time over the course of several minutes. Both BBI and ISAT efficiently sample and ionize surface-active compounds on liquid interfaces making them particularly attractive techniques for understanding the role of surface-active molecules in atmospheric chemistry.

Offline Analysis of Aerosol Samples. Although real-time measurements provide the most complete information about atmospheric processes, offline analysis is preferred in cases when it is impractical to bring the instrument to the measurement location or when time-averaged composition is needed. In such cases, particles are collected on filters and gases are collected on suitable sorbents, and the collection media are brought back to the lab for offline analysis. In this section, we summarize several important recent developments focused on improving the molecular speciation of OA constituents using established separation and MS analysis techniques.

High-Resolution Mass Spectrometry (HRMS). HRMS is a powerful tool for the molecular-level chemical analysis of OA. A common strategy in the analysis of aerosol samples collected on substrates involves extraction of the collected material into an appropriate solvent followed by either direct infusion or high-performance liquid chromatography (HPLC) HRMS analysis with ESI (HPLC-ESI-HRMS). The complexity of OA samples presents challenges for extraction, separation, and ionization of their components. Several recent studies have addressed some of these challenges. For example, it has been demonstrated that the extraction step can be selective toward surface-active compounds in aerosol samples.⁴³

Similarly, the ionization step may be optimized to preferentially ionize different classes of compounds. In one study, Cochran et al.⁴⁴ used atmospheric pressure chemical ionization (APCI) to characterize polycyclic aromatic hydrocarbons (PAHs) eluting from an HPLC column. In contrast to ESI, which is sensitive to polar molecules, APCI is well-suited for the analysis of nonpolar compounds such as PAHs. Commercially available PAH derivatives containing different functional groups (e.g., nitro, amino, carbonyl, carboxyl, hydroxyl) were analyzed to examine the types of molecular ions and fragments produced for different classes of PAHs in APCI. APCI spectra contained both intact protonated molecules, $[M + H]^+$, and molecular radical cations, $M^{+\bullet}$, in positive mode, $[M - H]^-$ species in negative mode, and fragment ions corresponding to losses of small molecules and radicals in both positive and negative modes. The relative abundance of different fragments was strongly dependent on the structure and composition of the precursor molecule. Experiments with standards provided the basis for the identification of molecules produced in heterogeneous ozonation of PAHs. In another study, Parshintsev et al.⁴⁵ employed desorption atmospheric pressure photoionization (DAPPI-HRMS) to analyze aerosol samples directly from quartz filters. In DAPPI, analyte molecules are desorbed from the substrate by a heated jet of solvent vapor and ionized by vacuum ultraviolet (VUV) photons from a krypton discharge lamp. A suitable dopant molecule is added to the spray solvent to assist ionization. Numerous oxidation products of terpenes have been observed in DAPPI-HRMS and tentatively identified based on their accurate m/z values. A path to the automated analysis of aerosol samples using DAPPI was discussed. It involves a moving belt, which will be used both for the collection and immediate DAPPI analysis of the collected samples with minimal delay.

GC-MS of Collected Particulate Matter. GC-MS continues to be extensively used for the offline characterization of OA. Recent developments in this field have been focused on improving the sensitivity, ease of use, and structural characterization of compounds in complex organic mixtures. In particular, several derivatization strategies specifically targeting OA compounds have been evaluated. For example, a single-step derivatization approach using *N*-methyl-*N*-trimethylsilyltrifluoroacetamide, trimethyl-chlorosilane, and pyridine was optimized for the analysis of common SOA tracers including pinic acid, pinonic acid, and 2-*C*-methyl-*D*-erythritol.⁴⁶ It was demonstrated that the derivatization temperature and time along with the amount of pyridine affect the limits of detection. The best values obtained under optimized conditions were in the range of 0.10–0.19 $\mu\text{g}/\text{mL}$. A different derivatization strategy employing *O*-(2,3,4,5,6-pentafluorobenzyl)hydroxylamine hydrochloride as a reagent was developed for the quantification of atmospheric carbonyl compounds.⁴⁷ The approach was evaluated using several representative carbonyl compounds including acrolein, benzaldehyde, glyoxal, methyl glyoxal, methacrolein, methyl vinyl ketone, and 2,3-butanedione. Optimization parameters included the extraction solvent, reagent concentration and solution pH during derivatization/extraction, and the time of both extraction and derivatization; detection limits of 0.01–0.17 $\mu\text{g}/\text{mL}$ were obtained under the optimized conditions. In a related study, a two-step derivatization approach involving oximation of analyte molecules followed by silylation was developed for the

simultaneous analysis of aldehydes and carboxylic acids in complex organic mixtures.⁴⁸

Two-dimensional GC (2D GC or GC \times GC) coupled with MS is a powerful technique for the analysis of environmental samples. The developments in this field have been summarized in a comprehensive review,⁴⁹ and only selected recent studies focused on the 2D GC analysis of OA will be briefly discussed here. In one study, Martinez et al.⁵⁰ used 2D GC to separate compounds based on their volatility in the first column and use a short polar GC column for subsequent polarity separation. A modulator installed before the second column acts as a preconcentration device, which dramatically improves the sensitivity of the system. High-resolution mass analysis using a TOF-MS system compensates for the relatively inefficient separation in the second (short) column. This novel experimental platform enables fast 2D GC analysis (15–30 min) with high sensitivity and provides additional information on the volatility and polarity of OA compounds of interest to atmospheric models.

In another study, Alam and Harrison used a variable energy electron impact (EI) ionization to distinguish and identify structurally related compounds, which produce similar fragmentation patterns in a traditional GC-MS experiment.⁵¹ This technique was used to identify relatively large (C_{12} – C_{36}) aliphatic and aromatic molecules in motor oil samples. By comparing EI spectra obtained at 14 and 70 eV, the authors were able to identify isomeric species. Mass spectral data combined with retention times provide insights into the structures of large molecules in complex organic mixtures. This approach was subsequently extended to the quantitative analysis of semivolatile organic compounds in diesel exhaust.⁵² Both gas phase and particle phase compounds including long-chain alkanes (C_{11} – C_{33}), cycloalkanes (C_{11} – C_{25}), decalins, C_9 – C_{12} aromatic and PAH compounds were identified in that study. Several classes of compounds including ketones, aldehydes, naphthalenes, and sulfur-containing species were observed exclusively in the gas phase. More than 12 000 peaks were separated in these complex samples using 2D GC. Low-energy (14 eV) ionization spectra were acquired to determine molecular masses of species not found in the NIST library. This enabled tentative identification of numerous previously unknown compounds in diesel exhaust. In a related study, Worton et al.⁵³ combined 2D GC with traditional 70 eV EI, vacuum ultraviolet (VUV) photoionization at 10.5 eV, and high-resolution TOF-MS for improved identification of compounds in OA. The combination of EI and VUV ionization methods improves confidence in identification of unknown organic compounds and provides more than twice as much molecular level peak information than EI alone.

High-Performance Liquid Chromatography Mass Spectrometry (HPLC-MS). Several studies focused on the development of advanced approaches for OA analysis using high- or ultrahigh-performance liquid chromatography (HPLC or UPLC, respectively) coupled to MS. For example, Ranney and Ziemann⁵⁴ introduced an approach for quantitative analysis of molecules in OA by combining derivatization with HPLC separation and detection of the eluting compounds using UV–vis spectroscopy and analysis of fractionated compounds using CIMS. Derivatization compounds were selected to enable accurate quantification of both mono- and multifunctional carbonyl, carboxyl, hydroxyl, and ester-containing species. Quantification using UV–vis detector was performed over 2–3 orders of magnitude in concentration with detection limits of

0.003, 0.02, 0.01, and 1 nmol for carbonyl, hydroxyl, carboxyl, and ester groups, respectively. Best CIMS data were obtained using isobutane as the reagent gas. Experimental artifacts resulting from carbonyl derivatization typically performed under highly acidic conditions (pH \sim 1) have been discussed. These include decomposition of peroxides and hydrolysis of hemiacetals, acetals, and esters that could contribute to oligomer decomposition. Other derivatization reactions are performed under mild conditions and are not expected to alter the distribution of functional groups in OA samples to a significant extent.

Because of the complexity of OA samples containing numerous classes of compounds, optimum separation in HPLC is challenging. Lin et al.⁵⁵ evaluated the ability of different columns to separate compounds in a well-studied atmospherically relevant organic mixture produced by reacting methylglyoxal (MG) with ammonium sulfate (AS). In particular, brown carbon (BrC) chromophores were characterized in that study by combining HPLC with a photodiode array (PDA) detector and ESI-HRMS detection (HPLC-PDA-ESI-HRMS), which enabled their separation both by the retention time and UV–vis absorption. Six different columns were evaluated and the best separation was achieved using the SM-C18 column while the least successful separation of this organic material was obtained using the HILIC (hydrophilic interaction liquid chromatography) column. The superior performance of the SM-C18 column was attributed to the nonpolar nature of compounds in the mixture. In addition, a combination of the reverse-phase interactions and ion exchange capability of the column proved to be advantageous for the separation of both protonated molecules and species that remain neutral at the pH of the separation solvent. In contrast, HILIC column provides superior separation of atmospherically relevant monosaccharide anhydrides (e.g., levoglucosan, galactosan, and mannosan).⁵⁶ These results indicate that careful selection of the HPLC column and separation conditions requires prior knowledge of the properties of OA compounds.

In many environments, primary biological aerosol particles (PBAP) contribute substantially to atmospheric aerosol, influencing both air quality and climate.^{57,58} Liu et al.⁵⁹ used HPLC-ESI-HRMS combined with MS/MS for identification of proteins in the ambient PBAP. In that study, the authors designed the experimental protocols for extracting and analyzing proteins from bulk filter samples of particulate matter. In samples collected at urban sites in central Europe, they detected proteins originating from plants, fungi, and bacteria and identified some of their atmospheric degradation products. This type of metaproteomic analysis of atmospheric aerosols is an attractive new tool for probing the composition and transformations of allergens in airborne PBAP, their spatiotemporal variability, and implications for human health.

MS Analysis of Individual Particles. Mass spectrometry has been extensively used for chemical analysis of both individual airborne and substrate-deposited particles. In particular, single-particle mass spectrometry (SPMS) enables real-time analysis of the chemical composition of airborne aerosols. Recent studies in this field have been focused on the design and evaluation of compact field-deployable SPMS systems,^{60,61} development of improved ionization approaches for a wider coverage of components in individual particles,⁶² development of orthogonal approaches for separation and comprehensive characterization of individual particles prior to MS analysis,⁶³ improving the optical detection efficiency of

individual particles,^{64,65} development of an aerodynamic lens for the online detection of airborne bacterial cells,⁶⁶ and application of statistical data analysis tools for clustering and efficient visualization of the experimental data.^{60,61,67}

Mardsen et al.⁶⁴ demonstrated that an order of magnitude improvement in SPMS sensitivity may be achieved by carefully designing the optical detection system. Furthermore, a substantially broader coverage of both PAHs and inorganic species in individual particles was reported by Passig et al.⁶² This was achieved by combining gentle particle desorption using an infrared (IR) laser with resonantly enhanced multiphoton ionization (REMPI) of PAHs using a 248 nm UV laser and laser desorption ionization (LDI) of inorganic compounds using a 193 nm VUV laser. In their method, the two ionization events are separated by a 2 μ s delay, during which positive ions produced by REMPI are extracted into a TOF-MS for analysis. LDI ions are subsequently analyzed in the second flight tube also operated in positive mode. A schematic drawing of the desorption/ionization sequence and representative mass spectra of two different particles obtained using this approach are shown in Figure 4. PAHs were observed as dominant peaks in REMPI spectra and show a different distribution for different particles. In addition, a soft wood combustion marker, retene, was observed at m/z 234 in the spectrum of a single wood ash particle. The LDI spectrum of the diesel exhaust particle was dominated by carbon peaks typical of soot particles while potassium was the dominant peak in the LDI spectrum of the wood ash particle.

The information content of the SPMS data may be enhanced through a detailed analysis of the physical properties of individual particles. For example, Alexander et al.⁶³ developed an experimental platform that enables simultaneous measurement of dynamic shape factors of individual ambient particles and their molecular composition. In this instrument, particles with a narrow distribution of masses are selected using an aerosol particle analyzer and their mobility diameters are measured using DMA. Particles are subsequently filtered based on their mobility diameters and molecular composition; aerodynamic diameters of individual particles are characterized using SPMS. The results demonstrated that mass- and mobility-selected particles were still present in different shapes as reflected by a distribution of their aerodynamic diameters. For quartz particles, this approach demonstrated that particles become more aspherical with an increase in size.

Although a majority of studies have been focused on airborne particles, recent developments in chemical imaging using mass spectrometry have opened up new opportunities for studying the properties of aerosols collected on substrates. Studies by Li et al.^{68,69} have established chemically selective imaging using NanoSIMS (secondary ion mass spectrometry with nanometer resolution) as a powerful tool for the quantitative mapping and speciation of nitrogen-containing compounds in individual particles collected on silicon nitride windows. NanoSIMS enables simultaneous mapping of several fragment ions produced using surface bombardment with a high-energy primary ion beam with a lateral resolution down to 50 nm and is, therefore, particularly attractive for chemical imaging of individual particles. Carbon, oxygen, and nitrogen mapping was achieved by measuring abundances of $^{12}\text{C}^-$, $^{16}\text{O}^-$, $^{12}\text{C}^{14}\text{N}^-$, and $^{14}\text{N}^{16}\text{O}_2^-$ secondary ions produced using Cs^+ primary beam and $^{14}\text{NH}_4^+$, $^{14}\text{NH}_3^+$, $^{14}\text{NH}_2^+$, and $^{14}\text{NH}^+$ fragments generated upon surface bombardment with O^- primary ions. Differentiation of nitrogen-containing compounds was performed

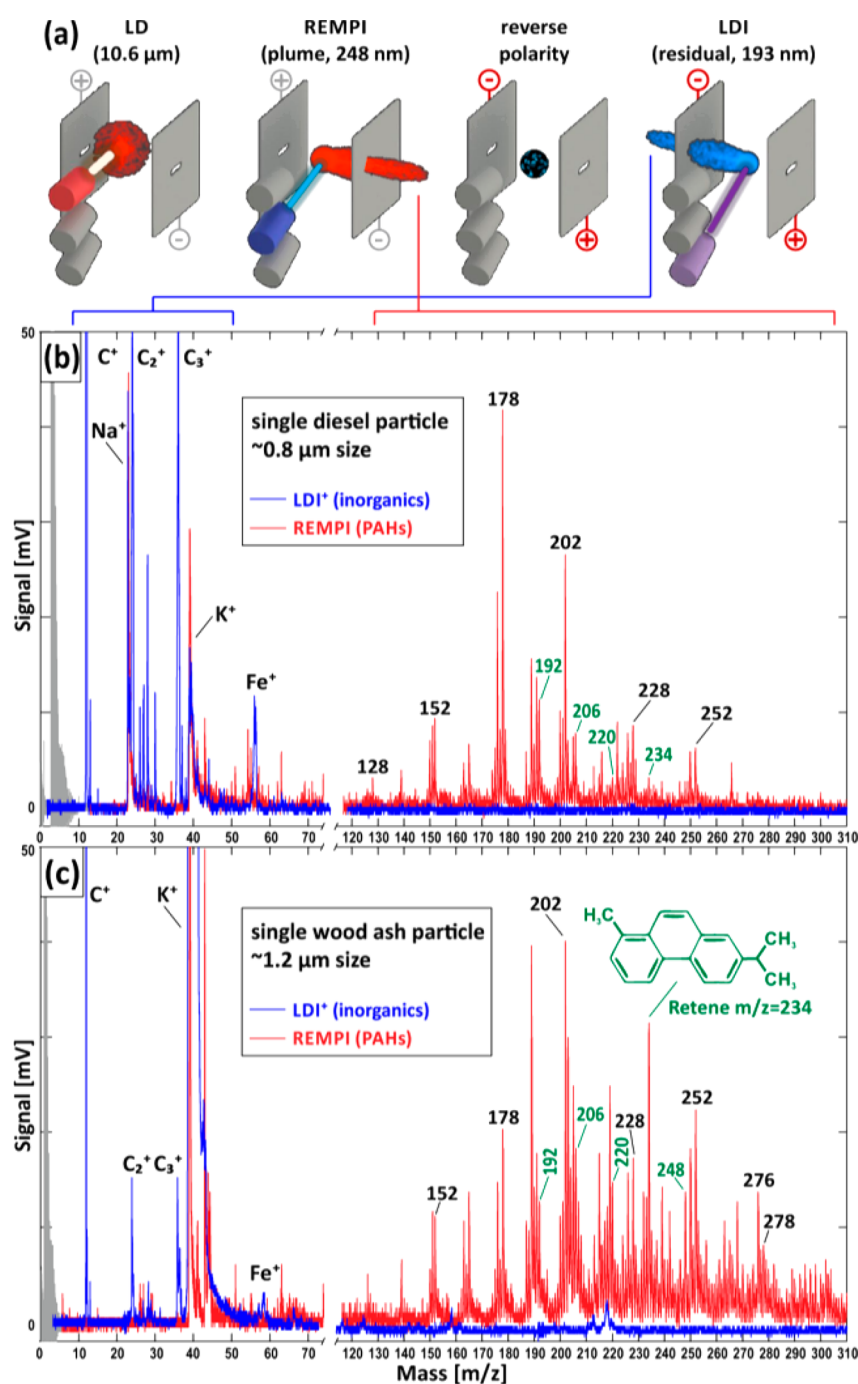


Figure 4. (a) Laser pulse sequence used in REMPI/LDI analysis of individual particles. (b) LDI⁺ (blue) and REMPI (red) mass spectra of a single diesel exhaust particle reveal a soot dominated particle containing predominantly nonalkylated polyaromatics (black m/z numbers). (c) Mass spectra from a single wood ash particle indicate a potassium-dominated core and a higher number of oxidized and alkylated PAHs. Note the wood combustion marker retene at $m/z = 234$. Green labels: row of alkylated phenanthrenes. Gray: noise from high-voltage switches. Reproduced from Passig, J.; Schade, J.; Oster, M.; Fuchs, M.; Ehlert, S.; Jäger, C.; Sklorz, M.; Zimmermann, R., *Anal. Chem.* **2017**, *89*, 6341–6345 (ref 62). Copyright 2015 American Chemical Society.

using three fragment ions: the $^{14}\text{N}^{16}\text{O}_2^-$ ion characteristic of nitrates and nitrites, the $^{14}\text{NH}_4^+$ ion specific to ammonium salts, and the $^{12}\text{C}^{14}\text{N}^-$ fragment of nitrogen-containing organic molecules. NanoSIMS images of particles containing a mixture of glucose and KNO_3 with different molar ratios are shown in Figure 5.⁶⁸ The results demonstrated phase separation of the organic and inorganic components during the drying process until the salt content decreased to <20%. Calibration plots were generated by examining ion abundances as a function of the

particle composition. Good correlation between the normalized ion abundances and carbon, oxygen, and NO_3 molar fractions demonstrated the potential of NanoSIMS for quantitative analysis of individual particles. For mixed organic/inorganic particles, NanoSIMS produced quantitative results for C, O, and NO_3 with $\pm 20\%$ error.⁶⁸ The accuracy obtained for pure inorganic particles composed on (NaNO_3 and KNO_3) was $\pm 1.9\%$.⁶⁹

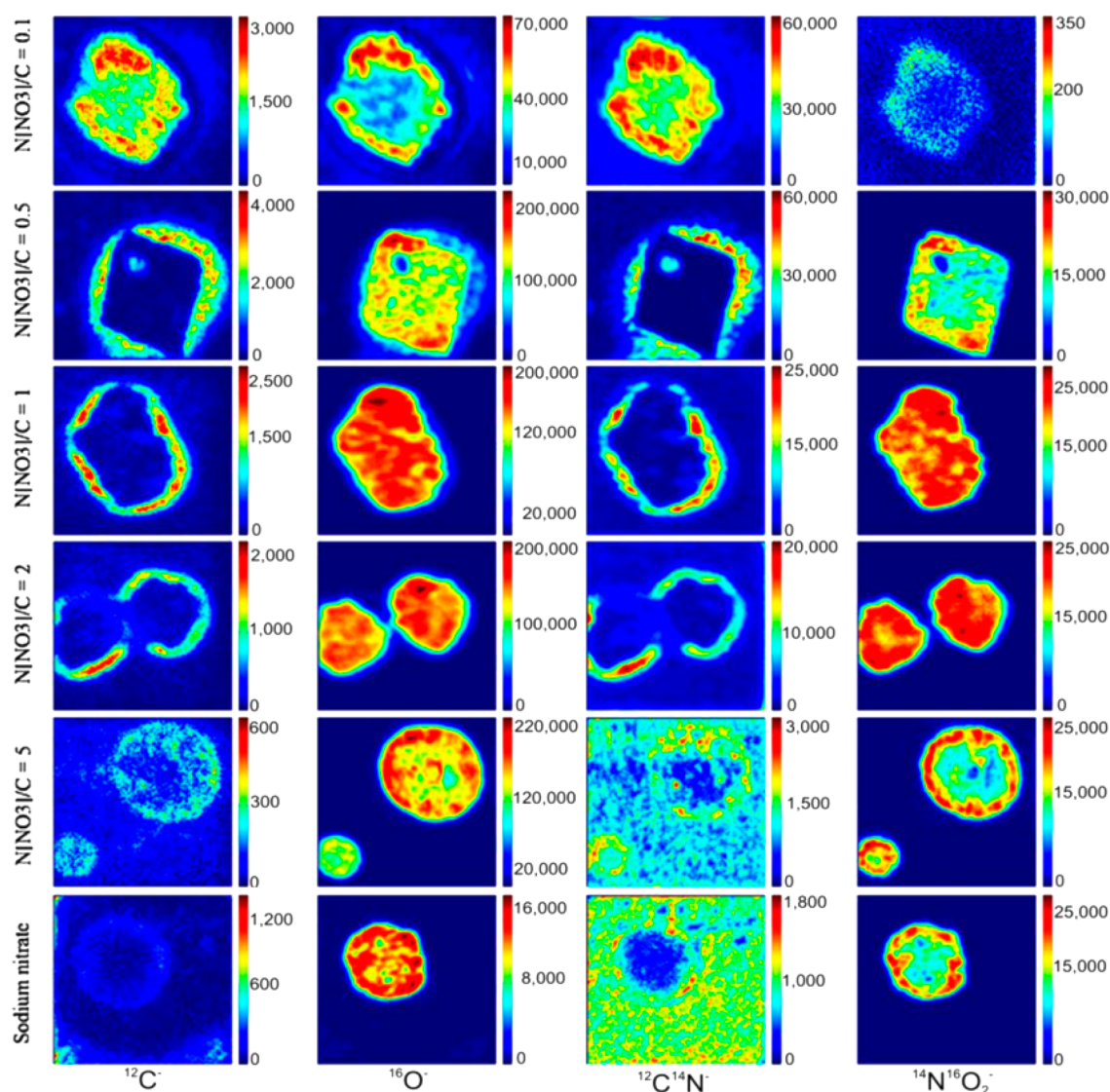


Figure 5. Negative secondary ion images of aerosol like mixture samples of KNO_3 mixed with glucose at different mixing ratios. Field of view is $5 \times 5 \mu\text{m}^2$. The color scale denotes the signal intensity in counts per pixel. Reproduced from Li, K. X.; Sinha, B.; Hoppe, P., *Anal. Chem.* **2016**, *88*, 3281–3288 (ref 68). Copyright 2016 American Chemical Society.

Aerosol Mass Spectrometry (AMS). AMS implemented using a TOF-MS analyzer (TOF-AMS) has been widely used in atmospheric measurements for more than a decade.⁷⁰ Recently, the AMS capabilities have been further extended to enable the characterization of refractory soot particles containing thin organic coatings.⁷¹ This was achieved using a tunable VUV synchrotron-based light source in the 8–14 eV range of photon energies, which enables soft ionization of molecules produced by 1064 nm laser vaporization of soot particles and particles containing a metal core. The results indicated that this technique is suitable for the analysis of organic coatings on top of inorganic seed particles that absorb 1064 nm light. A different soft desorption/ionization in AMS using a near-infrared (NIR) laser was combined with a bipolar TOF-MS by Kenseth and Petrucci.⁷² This approach was shown to generate intact $[M + H]^+$ and $[M - H]^-$ ions of analyte molecules in positive and negative mode spectra, respectively. The ionization efficiency in positive and negative modes was proposed to be correlated to the analyte proton affinity and gas phase basicity,

respectively. Single-compound limits of detection obtained in that study were in the picogram range.

■ ADVANCES IN LABORATORY AND FIELD APPLICATIONS

In this section, we present examples of applications of MS-based techniques to studies of atmospheric chemistry of gas-phase molecules, nucleating clusters, airborne particles and droplets in both field and laboratory settings.

Highly Oxidized Multifunctional Organic Compounds.

Recent developments in MS instrumentation have enabled exciting new discoveries about the reactive gas-phase intermediates and unusual products formed during VOC oxidation. For example, it has been demonstrated that highly oxidized multifunctional organic compounds (HOMs) appear promptly during the early stages of oxidation of certain VOCs by autoxidation mechanisms, and have a surprisingly large number of oxygen atoms, with O/C ratios often exceeding unity. Although the yields of HOMs are only a few percent,⁷³ their extremely low volatility makes them good candidates for

the organic species implicated in new particle formation and growth.

The CI-API-TOF-MS instrument with acetate ionization proved to be especially useful for the direct observation of HOMs in the gas phase. Remarkably, this instrument is capable of detecting not only closed-shell HOMs but also peroxy radical intermediates, RO₂, leading to HOMs. Furthermore, direct CI-API-ToF-MS detection of Criegee intermediates using protonated amines as reagent ions with a detection limit of 10⁴–10⁵ molecules/cm³ has been demonstrated.⁷⁴ The ability of CI-API-TOF-MS to directly observe reactive intermediates makes it possible to study the kinetics and mechanisms of reactions involving these species.

Richters et al.^{75,76} used a fast-flow tube reactor to study the formation of HOMs in ozonolysis of sesquiterpenes. Gas-phase products of VOC oxidation were probed using CI-API-TOF-MS a few seconds after mixing of VOC with ozone, before they could come in contact with the reactor walls. Reactions of sesquiterpenes with isotopically labeled ozone ¹⁸O₃ showed the presence of several competing mechanisms of HOM formation.⁷⁶ Specifically, the RO₂ radical produced through decomposition of the initial Criegee intermediate can either abstract a hydrogen atom from an aldehyde group or cyclize by reaction with the second double bond in the molecule. In a related study, Mentel et al.⁷⁷ used CI-API-TOF-MS to directly observe peroxy radical precursors of HOMs with 8–10 O atoms produced in ozonolysis of alkenes. They proposed that HOMs are multifunctional percarboxylic acids, with carbonyl, hydroperoxy, or hydroxy groups arising from the termination steps. Krechmer et al.³¹ examined HOMs derived from α -pinene using CI-IMS-MS. They showed that ion mobility separation prior to mass analysis makes it possible to distinguish isomeric HOMs formed by different reaction pathways.

The formation of HOMs does not appear to be limited to ozonolysis of alkenes. Berndt et al.⁷⁸ found that oxidation of isoprene by OH produces HOMs in reasonably high yields. For example, a compound with a formula (HO)₂-C₅H₈-(OOH)₂ was produced from isoprene with an estimated yield of 6%. OH oxidation of α - and β -pinene also was shown to produce HOMs.⁷⁹ The yields were of the order of a few percent, and they were higher for α -pinene derived HOMs. Importantly, the peroxy radical HO-C₁₀H₁₅(OO)(OOH)O₂ was observed not only in laboratory experiments but also during field measurements in Hyytiälä, Finland. In a combined theoretical and experimental study, Wang et al.⁸⁰ showed that oxidation of alkylbenzenes by OH can also produce HOMs. They observed HO-aromatic-(O₂)_x species with *x* up to 4 formed by the initial OH attack and followed by repeated addition of O₂ and intermolecular H atom shifts.

Although it is established that HOMs are produced in the early stages of gas-phase VOCs oxidation, their evolution in the atmosphere is still poorly understood. Zhang et al.⁸¹ reported the presence of highly oxidized C_{8–10}H_{12–18}O_{4–9} monomers and C_{16–20}H_{24–36}O_{8–14} dimers in particles produced through ozonolysis of α -pinene. They demonstrated that HOMs are readily detectable by positive-ion mode ESI as [M + Na]⁺ ions. The same compounds also were detected by iodide-CIMS in the gas phase providing evidence for gas-to-particle conversion of HOMs. Because of the large number of highly reactive hydroperoxy (-OOH) functional groups in HOMs, their lifetime in the particle phase is expected to be fairly short as they likely undergo secondary reactions with other particle-

phase compounds. Mutzel et al.⁸² examined SOA produced by ozonolysis of α -pinene under environmentally relevant precursor concentrations. They found that particles contained not only intact HOMs but also particle-phase decomposition products of HOMs and highly oxidized organosulfates. They hypothesized that highly oxidized organosulfates produced from HOMs may play an important role in particle growth due to their low volatility. Experiments by Krapf et al.⁸³ showed that HOMs are unstable in the particle phase and decompose under dark conditions with a half-life shorter than 1 h to produce H₂O₂ and organic acids. Because of their high reactivity, HOMs are expected to contribute to reactive oxygen species loading in particles and serve as precursors to free radicals by spontaneous decomposition and photochemical mechanisms.

New Particle Formation and Growth. A number of important studies focused on the new particle formation (NPF) and growth have been published in the time period highlighted in this review. A majority of these publications describe the ongoing work at the ultraclean CLOUD chamber at CERN.⁸⁴ A few selected examples from these studies demonstrating the role of MS in understanding the contribution of clusters and organic compounds to NPF will be provided below.

Clustering of sulfuric acid (SA) with ammonia or amines is recognized as a critical step in NPF. Kirkby et al.⁸⁵ presented experimental evidence of particle nucleation from HOMs in the absence of SA. Specifically, HOMs were produced by the ozonolysis of α -pinene in the CLOUD chamber at very low (0.01–1.3 ppbv) concentrations of α -pinene, something that would be very difficult to achieve in a conventional Teflon chamber. Two CI-API-TOF-MS instruments measured SA and HOMs concentrations in the chamber. The nucleation rates were measured under ion-free conditions and in the presence of ionizing radiation in the form of Galactic cosmic rays. A substantial increase in the nucleation rate by 1 to 2 orders of magnitude was observed in the presence of Galactic cosmic rays and attributed to ion-induced nucleation. MS characterization of the positively charged clusters clearly showed that ion-induced nucleation involves HOM dimers but not monomers (only peaks corresponding to compounds with 2, 4, 6, 8, and 10 monomer units in the cluster were observed), highlighting the importance of dimers in biogenic nucleation. Tröstl et al.⁸⁶ modeled the observed particle growth rates to obtain a better understanding of the factors affecting particle growth beyond the nucleation barrier. They predicted the saturation vapor pressures of HOMs observed in the chamber experiments using a functional group contribution method and showed that particle growth is initially driven by compounds with extremely low volatilities (saturation concentration <10^{-4.5} μ g/m³). Once the particles become large enough, compounds with higher saturation concentrations (10^{-4.5} to 10^{-0.5} μ g/m³) also start to contribute. Collectively, these two studies indicated that pure biogenic nucleation could be responsible for NPF in air masses depleted in SO₂. In a related study, Bianchi et al.⁸⁷ provided convincing observational evidence that at high altitudes, in a very clean air, NPF occurs mainly through condensation of HOMs with the conventional SA-NH₃ nucleation being a secondary process. This important conclusion was based on field measurements of nucleation rates and concentrations of key gas-phase species and clusters containing sulfate and nitrate anions along with HOMs at a high-altitude research station in Switzerland. The observed nucleation rates could not be adequately described using the SA-NH₃ mechanism alone.

However, the inclusion of HOMs enabled nearly quantitative prediction of the nucleation rates.

The importance of dimer compounds in the particle growth was demonstrated by Mohr et al.,⁸⁸ who examined dimers ($C_{16-20}H_{14-34}O_{6-9}$) produced through oxidation of monoterpenes in the boreal forest in Finland in both gas and particle phases using FIGAERO-CIMS. The observed concentrations (10^{-3} to 10^{-2} $\mu\text{g}/\text{m}^3$) of dimeric species were orders of magnitude higher than their estimated saturation concentrations (10^{-15} to 10^{-6} $\mu\text{g}/\text{m}^3$) strongly suggesting that they are formed by gas-phase processes (as opposed to dimerization of monomers in the particle-phase). Furthermore, gas-phase and particle-phase compounds with the same formula exhibited different diurnal patterns. The authors assessed the importance of dimers for the particle growth using the Model for Acid-Base chemistry in NANoparticle Growth (MABNAG). The dimers formed in the gas phase were predicted to contribute about 5% of the particle mass by the time the particle grew to 60 nm. The authors noted that the dimers observed in their study had O/C ratios lower than HOMs and probably were not produced via known autoxidation pathways. Instead, reactions of stabilized Criegee intermediates and RO_2 self-reactions were proposed to contribute to their formation. Vogel et al.⁸⁹ reached a similar conclusion that particle growth is driven by condensation of semi- and low volatility organic species formed by the gas-phase oxidation processes. They performed negative ion mode APCI-MS analysis of VOCs and offline UHPLC-ESI-HRMS analysis of the particle phase to determine the elemental composition of organic molecules before, during, and after NPF events at a rural mountaintop station in central Germany. Particles grew to larger diameters when extremely low-volatility organic compounds, presumably produced through sesquiterpene oxidation, started to dominate the spectrum. The primary contributors to the growth were CHO species (i.e., compounds containing only carbon, hydrogen, and oxygen atoms). Meanwhile, the measured abundances of CHON, CHOS, and CHONS compounds were not correlated with the active NPF events.

Lehtipalo et al.⁹⁰ examined the growth rate of sub-3 nm particles in the CLOUD chamber, in the presence of SA, water, NH_3 , and dimethylamine. In these experiments, neutral clusters consisting of multiple SA and dimethylamine molecules were detected using nitrate-CIMS. For a given SA concentration, the particle growth rate is known to increase in the presence of NH_3 and increase even further in the presence of dimethylamine. This growth rate enhancement is attributed to the formation of small acid-base clusters, which are typically not accounted for in measurements of SA concentration. Although the overall growth of particles is determined primarily by SA, the growth mechanism switches from the one driven by monomer-cluster collisions at low concentrations of basic gases to a different mechanism initiated by cluster-cluster collisions at sufficiently high concentrations of basic gases. The charge-induced enhancement of growth is important at the lowest particle sizes and low concentrations.

Lawler et al.⁹¹ examined the composition of 10 nm particles formed in the CLOUD chamber containing atmospherically relevant levels of gas-phase SA, dimethylamine, and traces of NH_3 using Thermal Desorption Chemical Ionization Mass Spectrometry (TD-CIMS). Despite the fact that the molar amount of basic gases in the chamber was higher than that of SA, the average particle composition showed lower than 1:1 base/acid ratio expected for partial neutralization and far lower

than the 2:1 ratio expected for complete neutralization of SA by the base. This indicates that once the particle is nucleated, SA does not require stabilization by NH_3 or dimethylamine in order to remain in the particle. Furthermore, even though dimethylamine is expected to be more effective as a stabilizing base for SA, at particle sizes around 10 nm and greater, NH_3 is taken up by the particles with comparable or even greater efficiency than dimethylamine.

Gas-Phase Oxidation of VOC and SOA Formation.

HRMS coupled with different ionization sources and separation stages enables advanced molecular level characterization of SOA formed through the oxidation of VOCs both in controlled laboratory experiments and in ambient environment. These methods have been used to obtain unique mechanistic insights into both VOC oxidation and SOA formation and transformations in the atmosphere. For example, Duporte et al.^{92,93} used a combination of the online TOF-CIMS and offline HPLC-ESI-HRMS methods to study α -pinene ozonolysis in the presence of dimethylamine which was found to enhance new particle formation and SOA growth. Several low-volatility nitrogen-containing products of reactions between dimethylamine and pinonaldehyde or pinonic acid were identified in both laboratory and boreal forest samples indicating their potential contribution to SOA formation in the atmosphere. Rindelaub et al.⁹⁴ used a combination of GC-MS, HPLC-MS, and paper spray MS to examine both gas-phase and condensed-phase products of OH-initiated α -pinene oxidation under high NO_x conditions. Over 30 compounds including pinocamphe-
nol, fencholenic aldehyde, and α -pinene-derived nitrate isomers were identified in that study. Lee et al.⁹⁵ used FIGAERO TOF-CIMS instrument to probe nitrogen-containing organic compounds in both gas and particle phases in a forested environment near Centerville, AL. They identified a new class of highly functionalized, low-volatility nitrogen-containing organic molecules and showed that these species make a dominant contribution to the total particle nitrate mass measured by traditional AMS. Modeling results suggested that these particle-phase organic nitrates are likely produced through oxidation of biogenic VOCs and have short lifetimes (of the order of a few hours) in the particle phase. The mechanism of their rapid loss could not be established with certainty. One of the important implications of the short lifetime is that partitioning of low-volatility organic nitrates into the particles followed by their decomposition in the particle phase may be an important process contributing to SOA formation in the atmosphere. Furthermore, the dynamic partitioning of organonitrates between gas and particle phases may modify the cycling of gas-phase NO_x in yet unrecognized ways.

MS also has been used to examine uptake of oxidized VOCs onto ambient particles. For example, reactive uptake of IEPOX onto acidic aerosol was studied by Riva et al.⁹⁶ using Single-Particle Laser Ablation Time-of-Flight-Mass Spectrometry (SPLAT-MS).⁹⁶ It is known that reactive IEPOX uptake producing organosulfates and methyltetrols is a major process contributing to the formation of isoprene-derived SOA. Using SPLAT-MS, the authors examined the effect of organic coatings of α -pinene SOA on the reactive uptake of IEPOX onto acidic ammonium bisulfate particles. They observed volume-limited uptake of IEPOX by ammonium bisulfate particles and reported that a thin coating of α -pinene SOA on the inorganic seed impeded the uptake.

Gallimore et al.^{97,98} used EESI-HRMS to examine changes in SOA composition during ozonolysis of oleic acid⁹⁷ and limonene⁹⁸ in real time. The ions detected with EESI-MS in limonene SOA samples compared well with major products identified in previous offline ESI-MS studies. Time-resolved data acquired for numerous products of oleic acid oxidation, including short-lived stabilized Criegee intermediates, secondary ozonides, stable primary oxidation products, and oligomers, showed that a majority of these species were formed through nonfirst-order reactions. A process-level model was then used to interpret a subset of these measurements, which allowed constraining the relative rates of secondary reactions of individual compounds formed in the ozonolysis of oleic acid. The results indicated that ozone oxidation of the oleic acid occurs predominately on the particle surface and that reactions with 9-oxononanoic acid are the major sink for Criegee intermediates in the particle phase.

Kourtchev et al.⁹⁹ used direct infusion ESI-HRMS analysis of SOA samples collected on filters to examine the relative yield of oligomer formation as a function of SOA mass. They found that the fraction of oligomers produced through the oxidation of VOC increases with SOA mass. The relative abundances of oligomeric compounds were higher in samples prepared at high VOC concentrations. This important result may help resolve a long-standing discrepancy between observations of the large fractions of oligomers in laboratory experiments and modest oligomer fractions detected in field samples.

ESI-HRMS has been used to examine the molecular composition of ambient OA. For example, Tong et al.¹⁰⁰ used ESI-HRMS for molecular characterization of vehicle exhaust particles sampled in a road tunnel and mixed POA/SOA particles at an urban site in Birmingham, U.K. A high number of monoaromatics and oxygen- and nitrogen-containing PAH species were detected in the tunnel samples and many nitro-aromatic compounds were identified. In contrast, S-containing species were more abundant in OA samples collected at the urban site, suggesting their formation through secondary processes and aging through reactions with sulfate and SA. Willoughby et al.¹⁰¹ examined the composition of ambient OA produced by major sources (marine, biomass burning, urban emissions) using a multimodal molecular characterization approach that combines HRMS and ¹H NMR spectroscopy. This combination of a detailed molecular coverage provided by HRMS and functional group information from ¹H NMR measurements helps identify important classes of OA components. This study provided a clear evidence of the presence of biomolecules (lipid-like compounds) in marine OA and nitrogen-containing aromatic compounds in BBOA. Urban OA was found to contain a substantially more oxidized and structurally diverse mixture of organic species consistent with the diversity of sources and more extensive atmospheric aging.

Blair et al.¹⁰² used complementary capabilities of AMS, nanospray desorption electrospray ionization (nano-DESI)/HRMS, and ultrahigh resolution and mass accuracy 21 T FTICR (Fourier-transform ion cyclotron resonance) MS to characterize OSCs including organosulfates $-\text{OS}(\text{O})_2\text{OH}$ and sulfonates $-\text{S}(\text{O})_2\text{OH}$ in SOA formed in photooxidation of diesel fuel in the presence of SO_2 . The results showed that yields of OSCs increased with the SO_2 concentration under dry conditions (Figure 6). However, the yield of OSCs dropped when SOA photooxidation took place at an elevated relative humidity. Substantial overlap between OSCs observed in the laboratory settings and field data was reported. It was suggested

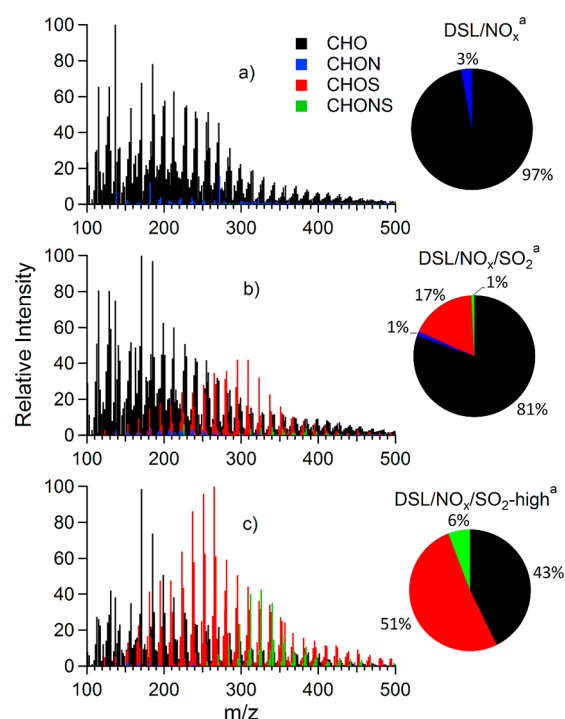


Figure 6. Nano-DESI-HRMS spectra of diesel fuel SOA (DSL) showing the effect of SO_2 addition on the aerosol composition (a) no SO_2 , (b) 200 ppbv SO_2 , (c) 570 ppbv SO_2 . Peaks are colored by the elemental composition. Pie charts show intensity weighted fractions of the peaks. Reproduced from Blair, S. L.; MacMillan, A. C.; Drozd, G. T.; Goldstein, A. H.; Chu, R. K.; Pasa-Tolic, L.; Shaw, J. B.; Tolic, N.; Lin, P.; Laskin, J.; Laskin, A.; Nizkorodov, S. A., *Environ. Sci. Technol.* **2017**, *51*, 119–127 (ref 102). Copyright 2017 American Chemical Society.

that many molecules in field-collected samples that were originally assigned to organosulfates from biogenic precursors likely originate from anthropogenic sources, such as photooxidation of diesel and biodiesel fuel.

HPLC-ESI-HRMS has been extensively used for the identification of organosulfates in SOA. For example, Duporte et al.¹⁰³ identified organosulfates produced in reactions between acidified ammonium sulfate particles and selected primary products of α -pinene oxidation (α -pinene oxide, isopinocampheol, pinanediol, and myrtenal). Reaction of α -pinene oxide showed the highest yield of organosulfate production. Consistent with the observations of Blair et al.,¹⁰² the reaction was suppressed at higher humidity. Riva et al.¹⁰⁴ studied aliphatic organosulfates in SOA produced by photooxidation of C_{10} – C_{12} alkanes. Organosulfates identified in that study were likely formed through acid-catalyzed reactive uptake of gaseous epoxides onto acidified sulfate particles or through heterogeneous reactions of hydroperoxides. Some of the organosulfates observed in laboratory-generated SOA were also detected in field samples collected from Lahore, Pakistan, and Pasadena, CA. Barbosa et al.¹⁰⁵ studied organosulfates in SOA produced from *cis*-3-hexen-1-ol (a green leaf VOC emitted by plants under stress) in the presence of seed sulfate particles. A number of precursor-specific organosulfates detected in laboratory experiments were subsequently identified in SOA samples collected in Rio de Janeiro, Brazil.

Brüggemann et al.¹⁰⁶ used a combination of MS techniques with different ionization and sampling methods for the real-time detection of organosulfates in ambient OA in central

Europe. Specifically, aerosol composition was examined using aerosol flowing atmospheric-pressure afterglow (AeroFAPA) MS, AMS and CI-APi-TOF-MS. In addition, offline analysis of collected OA samples was performed using HPLC-ESI-HRMS. The study demonstrated the abundance of various types of organosulfates, nitrooxy organosulfates, and highly oxidized organosulfates in ambient OA. Systematic correlations between highly oxidized organosulfates, sulfate, and HOMs reported in that study indicate that highly oxidized organosulfates are likely formed through gas-phase reactions of HOMs with sulfate particles. Using a combination of AMS with APCI-MS, Vogel et al.¹⁰⁷ provided experimental evidence that particle hygroscopic properties may be affected by the presence of nitrooxy organosulfates. Specifically, they observed a measurable decrease in hygroscopicity for particles containing substantial amounts of organosulfates and reported that hygroscopicity increases with photochemical aging.

Aqueous-Phase SOA Chemistry. Two distinctly different types of aqueous phases exist in the atmosphere. The first one represents liquid water present in fine (diameter $<2.5 \mu\text{m}$) and coarse (diameter $<10 \mu\text{m}$) particles known as “aerosol liquid water” (ALW). Under ambient RH, ALW may account for several tens of percent of volume of hygroscopic particles. This is sufficient to dissolve most water-soluble particle compounds resulting in a highly concentrated solution of both organic and inorganic compounds. The reactions occurring in ALW are often driven by its high acidity (pH <3). The second type of aqueous environment is found in cloud and fog droplets, which are considerably more dilute than ALW and typically far less acidic (pH = 4–6). Both types of aqueous phases can sustain photochemical and dark reactions converting volatile water-soluble compounds into more oxidized and less volatile compounds, which are collectively called aqSOA¹⁰⁸ to emphasize their aqueous chemistry origin.

Several recent field studies provided compelling evidence for aqSOA formation in the atmosphere. For example, Sareen et al.¹⁰⁹ examined the abundance of water-soluble compounds in Brent, Alabama, during SOAS. They scrubbed ambient air using a mist chamber, spiked the resulting solutions with H_2O_2 , and exposed them to UV radiation to generate OH and initiate radical chemistry. The products of these aqueous phase reactions were analyzed using direct infusion ESI-HRMS and tandem mass spectrometry (MS/MS). Formation of pyruvate, oxalate, and acetate/glycolate through aqueous photooxidation reactions was observed. The authors noted that these acids are too volatile to remain in acidified particles. However, they would be retained in the particle phase in the presence of ammonia, when particles are more neutralized. Sullivan et al.¹¹⁰ found evidence for ambient dark aqSOA formation during the PEGASOS (Pan-European Gas-AeroSols climate interaction Study) 2012 campaign in the Po Valley, Italy. They performed a factor analysis of TOF-AMS data and observed dark formation of WSOC with a high average level of oxidation (based on the O/C ratio). A correlation of WSOC with ALW and nitrate was observed during times of increasing RH. In what is arguably the strongest field observation evidence for aqSOA formation published during the review period, Gilardoni et al.¹¹¹ observed aqSOA formation in both fogwater and in ALW via aqueous-phase processing of biomass-burning emissions in the Po Valley using TOF-AMS.

Faust et al.¹¹² examined the effect of ALW on the yield and composition of SOA produced by ozonolysis of α -pinene, photooxidation of toluene, and photooxidation of acetylene.

The reaction was carried out in a flow tube in the presence of the same amount of either aqueous or solid ammonium sulfate seed particles, and the products were analyzed by TOF-AMS. In all cases, the presence of ALW enhanced the observed SOA yields. The effect of ALW was especially pronounced for SOA formed through acetylene photooxidation, which generates a highly water-soluble glyoxal as a product. The authors concluded that ALW plays a complicated, system-dependent role in SOA formation and is especially important for photooxidation systems that produce volatile but soluble carboxylic acids and carbonyls.

Lim et al.¹¹³ used UPLC-TOF-MS to examine products of dark and photochemical oxidation of glyoxal in the presence of ALW in deliquesced ammonium sulfate or sulfuric acid particles and in the presence of NO_x and ozone. In addition to the expected oxalic and tartaric acid, the major observed products were organonitrogen (CHNO), organosulfur (CHOS), and mixed compounds (CHNOS). Some of the CHNO compounds were identified as nitric acid esters. These compounds are likely produced via nonradical reactions of glyoxal with nitric acid present in the aqueous phase. Several unusual organosulfur species also were observed. For example, a compound with a formula $\text{C}_2\text{H}_2\text{O}_8\text{S}_2$ was proposed to be formed through a condensation reaction of monohydrated glyoxal with two sulfuric acid molecules. These chemical pathways, some of which have not been previously reported, may play an important role in urban air under humid conditions.

Aqueous photochemistry of suspended droplets ($\sim 1 \mu\text{m}$ in diameter) containing dissolved iron oxalate, glycolaldehyde, and ammonium sulfate at pH ~ 3 (representative of ALW) was examined by Thomas et al.¹¹⁴ using field-induced droplet ionization mass spectrometry (FIDI-MS). Upon exposure to 365 nm radiation, glycolaldehyde was found to undergo oxidation to form glyoxal, glycolic acid, and glyoxylic acid. In both droplet and smog chamber experiments, in which glycolaldehyde reacted with wet aerosol particles under irradiation, the presence of iron suppressed the formation of high-molecular weight products of glycolaldehyde oxidation. The results demonstrate that even trace amounts of soluble iron can strongly impact the composition of aerosol produced by aqueous photochemistry.

MS also has been used in several laboratory studies to identify products of OH oxidation and direct photolysis of WSOC in bulk aqueous solutions. For example, Renard et al.¹¹⁵ used a traveling wave IMS-MS coupled to an ESI source and UPLC to examine oligomeric compounds produced by aqueous-phase OH oxidation of methyl vinyl ketone and other unsaturated water-soluble compounds (methacrolein, ethyl vinylketone, methacrylic acid, fumaric and maleic acids, etc.). For methyl vinyl ketone, they observed oligomers containing up to 14 monomer units. In general, they found that precursor compounds with one double bond or two nonconjugated double bonds did not undergo oligomerization indicating the important effect of the structure of atmospheric precursors on their aqueous chemistry.

Aqueous photolysis of glyoxylic¹¹⁶ and pyruvic acid¹¹⁷ was studied by Eugene et al. using a number of analytical methods, which included direct infusion ESI-HRMS as well as UHPLC and ion chromatography coupled to MS. On the basis of the identified products, they proposed detailed mechanisms and suggested that the atmospheric photochemistry of abundant α -ketocarboxylic acids may trigger aqSOA formation. Rapf et

al.¹¹⁸ examined the mechanism of oligomer formation in aqueous photochemistry of pyruvic acid using negative ion mode ESI-MS. Even at the lowest concentrations (0.5 mM), pyruvic acid was observed to photodimerize generating parapryruvic acid and an array of other products. The dimer compounds were shown to undergo further photochemistry leading to trimer species. Lim and Turpin observed the formation of organic peroxides and peroxyhemiacetals in aqueous photooxidation of methylglyoxal using ESI-HRMS.¹¹⁹ The formation of peroxides has important implications for the recycling of OH in aqueous photochemical reactions.

Yu et al.¹²⁰ examined two mechanisms of aqSOA formation from phenolic compounds: reaction with a triplet excited state of an aromatic carbonyl and reaction with OH. Nano-DESI was used to observe time-resolved evolution of aqSOA mass, elemental ratios, and average carbon oxidation state. The results indicate that oligomerization is an important photooxidation pathway for phenolic compounds during the initial stages, followed by further oxidation and eventual fragmentation of the initially formed oligomers. Fragmentation reactions were found to eventually dominate the transformation of aqSOA, forming various highly oxygenated ring-opening products with carbon numbers below six. Aljawhary et al.¹²¹ reached similar conclusions in their experiments on aqueous photooxidation of cis-pinonic and tricarballylic acids using Aerosol-TOF-CIMS. A large number of reaction products were detected in these experiments suggesting a complex series of functionalization and fragmentation processes.

In addition to examining chemical transformations of water-soluble compounds leading to aqSOA, several studies focused on understanding mechanisms of aqueous aging of SOA compounds produced by gas-phase oxidation. For example, Zhao et al.¹²² prepared model SOA by ozonolysis of α -pinene, dissolved it in water, and observed rapid disappearance of dimeric compounds through aqueous reactions with OH. Using Aerosol-TOF-CIMS with iodide, acetate, and hydronium ion reagent ions, they directly observed decay in signals of C₁₆H₂₄O₈ (pinyl-diaterbyl ester), C₁₇H₂₆O₈ (pinyl-diaterpenyl ester), C₁₉H₂₈O₇ (pinonyl-pinyl ester), and several other prominent dimer compounds. Similarly, Romonosky et al.^{123,124} observed photodegradation of high-MW compounds after exposure of aqueous solutions of different types of SOA to UV light. Alkyl nitrates appeared to be most susceptible to photodegradation indicating that this process also is strongly affected by the structure of aqSOA compounds. These observations suggest that production of aqSOA from smaller water-soluble molecules may be counteracted by efficient fragmentation of larger SOA compounds.

Tong et al.¹²⁵ made an important observation that dissolution of SOA in water gives rise to OH radicals without any UV irradiation. The presence of OH was detected indirectly using spin-trapping agent, 5-*tert*-butoxycarbonyl-5-methyl-1-pyrroline-*N*-oxide (BMPO). The BMPO–OH adduct was observed by electron paramagnetic resonance spectroscopy and by HPLC-MS/MS. The molar yield of radicals from SOA formed by ozonolysis of α -pinene, β -pinene, and limonene was about 0.1% in pure water, but it increased to 1.5% in the presence of dissolved Fe(II) ions due to dark Fenton reactions. The authors estimated the OH production rate from SOA dissolved in cloud droplets as well as in the lung lining fluid of people inhaling polluted air. They concluded that the rate of OH formation by this mechanism is comparable to the rate of

Fenton process (Fe(II) + H₂O₂). In a related study, Tong et al.¹²⁶ examined aqueous mixtures of SOA and mineral dust particles, which can serve as a source of soluble iron. They found that substantial amounts of reactive oxygen species (ROS) including OH can be formed in aqueous mixtures of SOA and different types of mineral dust. They suggested that both the chemical reactivity and rates of aqSOA aging can be enhanced by interactions between SOA compounds and mineral dust in deliquesced particles and aqueous droplets.

Chemical Aging of Organic Aerosols. MS continues playing an important role in understanding changes in aerosol chemical composition pertinent to their atmospheric lifetime and aging. Using synchrotron based VUV-SP-AMS, Browne et al.¹²⁷ studied photooxidation of soot particles coated with organic layers in the presence of OH radicals. They showed that although soot particles remain largely unchanged after irradiation, organic molecules adsorbed on the soot surface age much faster than expected based on their photooxidation rates in the bulk or in purely organic particle phase. In a follow up study, Lim et al.¹²⁸ reported similar observations for oxidation of squalene films of variable thickness on soot and mineral dust particles. They found that the reaction rate constant had a linear dependence on the organic surface area-to-volume ratio with the rate constants for coated particles being up to 10 times higher than for pure particles. These results suggest that past experiments on oxidation of pure compounds, in aerosol or bulk form, may underestimate the atmospheric rates of oxidation. Another important conclusion from these studies is that the chemical composition at the particle surface changes much more rapidly for viscous particles in which the particle mixing time is very long.

Cheng et al.^{129,130} compared fragmentation and functionalization in heterogeneous reactions of tartaric acid + OH¹²⁹ and succinic acid + OH¹³⁰ using DART-MS. Structural characterization of the reaction products reported in these studies was used to elucidate common reaction mechanisms, allowing predictive understanding of the identity and locations of functional groups in the products of other carboxylic acids undergoing similar heterogeneous reactions. In a related report, Kroll et al.¹³¹ compiled the results of other studies involving OH-initiated oxidation of single-component organic particles explored using DART-MS and VUV-SP-AMS. They predicted that fragmentation and volatilization of the particle-phase constituents may result in 3–13% loss of OA carbon to the gas phase after 1 week of atmospheric oxidation. This confirms an old hypothesis that oxidative aging is an important sink for particulate organic carbon. The paper also introduced a concept of a carbon lifetime (molecular lifetime normalized to the number of C atoms in a molecule) to provide a parametrized description of the oxidative aging that is not tied to specific molecules. A variety of model OA systems examined in that study exhibited similar dependence of the fraction of carbon remaining on the carbon lifetime. This uniform dependence offers practical approach for the parametrization of the OH-driven aging in models.

Kourtchev et al.¹³² investigated the molecular composition and aging of SOA produced from a mixture of four biogenic volatile organic compounds (BVOC) using direct-infusion ESI-HRMS. They selected the relative molar fractions of BVOCs (40% α -pinene, 30% Δ_3 -carene, 20% β -pinene, and 10% isoprene) to represent the values typically observed in boreal forests. The resulting SOA was subsequently subjected to three aging scenarios in the chamber: dark reaction with residual

ozone, combined exposure to UV irradiation and OH radicals, and UV irradiation only. Of these three aging scenarios, only OH radical-initiated aging was found to influence the molecular composition and resulted in substantial increase of the average oxidation state of the aged SOA. Romonosky et al.^{123,124} used a similar HRMS platform to explore effects of different oxidation conditions on the molecular composition and aqueous photochemistry of SOA formed from α -pinene and α -cumulene. They reported substantial differences in the SOA composition formed under different conditions, which had subsequent effects on the stability of SOA under photolysis and hydrolysis processes. Oligomeric compounds were found to degrade faster than monomers resulting in faster evaporation of aged SOA particles in comparison with freshly formed SOA. The slow photodegradation of SOA observed by Kourtchev et al. in comparison with the faster photodegradation observed by Romonosky et al. suggest faster decomposition of SOA compounds in aqueous solutions (e.g., when dissolved in cloud droplets) in comparison with the particle phase. Support for this conclusion was provided by Hinks et al.,¹³³ who observed that certain photochemical processes can be impeded by the high viscosity of organic particles.

Volatility and Viscosity of Organic Aerosols. Many recent studies used new developments in MS instrumentation to provide insights on the viscosity and phase of aerosol particles, their implications for atmospheric chemistry, climate, and air quality. In one study, Lopez-Hilfiker et al.²⁵ used FIGAERO-CIMS to classify particle-phase products of α -pinene ozonolysis by their volatility and concluded that 50% of SOA compounds have vapor pressures much below those of monomeric oxidation products. They presented an experimental framework for correlating signals in the “thermogram” (i.e., mass spectra recorded as accumulated SOA material is slowly desorbed from the substrate) with the corresponding volatility ranges of SOA compounds based on the desorption temperature. The correlation provides a consistent view of SOA volatility and composition and helps improve the agreement between the measured and modeled gas-particle partitioning of SOA components.

Li et al.¹³⁴ introduced a parametrization method called “molecular corridors” for converting a set of molecular formulas and their peak abundances observed in HRMS experiments into the distribution of saturation mass concentrations (often called volatilities). The parametrization was initially used to estimate volatilities of compounds found in BBOA¹³⁵ and laboratory generated SOA.¹²⁴ The major challenge that prevents a broader application of this method is that it is difficult to convert the observed peak abundances in the mass spectrum into relative concentrations of the molecules in the sample. Currently, “molecular corridors” parametrization relies on the assumption that relative peak abundances adequately represent relative mass concentrations. Although this assumption is likely a good first approximation, development of robust approaches for calibrating peak abundances in HRMS is key to accurate evaluation of molecular volatilities based on HRMS data.

Online analyses of individual particles and their ensembles were used in a number of studies to investigate complex processes of transport and gas-particle chemistry in the aerosolized systems. Using SPLAT-MS, Bell et al.¹³⁶ examined the diffusion of NH_3 in α -pinene SOA on an individual particle basis. They found that at dry conditions, the reaction products form a few nanometer thick crust on the particle surface, which

limits further diffusion of NH_3 . This coating additionally prevents coagulating particles from coalescing on a time scale that exceeds 2 days. Using DART-MS, Chim et al.¹³⁷ showed that particles composed of 2-methylglutaric acid (2-MGA) are oxidized by OH more slowly at lower RH and that this is a viscosity (physical) effect as opposed to the chemical effect of ALW. Davies and Wilson observed that OH-induced oxidation of citric acid particles at low RH is limited to the particle surface.¹³⁸ For example, product formation was shown to occur over a narrow region near the particle surface, of the order of 8 nm at 20% RH.

Direct saturation vapor pressure measurements for representative organic compounds remain limited because of the difficulties associated with quantitative measurements of gas-phase concentrations at low partial vapor pressures. Bannan et al.¹³⁹ used Knudsen Effusion Mass Spectrometry for direct measurements of saturation vapor pressures of various phenolic and nitro-aromatic compounds relevant to anthropogenic organic aerosol. They showed that the measured values are orders of magnitude lower than the values obtained using existing approaches for estimating vapor pressure based on the molecular structure and composition. Similarly Huisman et al.¹⁴⁰ reported that the vapor pressures of compounds containing multiple carboxylic acid and other functional groups are much lower than previously reported. Wania et al. re-examined the data published by Bannan et al. and published a comment stating that a quantum-chemistry based method for predicting vapor pressures implemented in a commercial software called COSMOtherm gives much better agreement between the predicted and measured values; this comment was followed by a response by Topping et al.^{141,142} The large discrepancy in the measured saturation vapor pressures and the active polemics about the interpretation of the measurements highlight further need for more accurate measurements for representative particle-phase organic compounds.

Hinks et al.¹³³ studied the effects of viscosity on photodegradation of photolabile organic molecules embedded in a film of SOA material. In that study, HPLC-PDA-ESI-HRMS was used for the analysis of the photodegradation products. The study showed that photoreduction of 2,4-dinitrophenol, a common chromophore in anthropogenic OA, slowed down at lower temperatures and/or lower relative humidity, i.e., conditions that make the OA material more viscous and hinder molecular motion. The impeding effect of viscosity on the rate of photochemical processes is likely to be important whenever the reaction rate is limited by diffusion of the electronically excited molecule toward its reaction partner.

Chemistry of Brown Carbon. Molecular characterization of light-absorbing components in organic aerosol (brown carbon or BrC)^{6,143} has been substantially advanced in recent years through applications of HPLC-PDA-ESI-HRMS. This method was utilized in a number of field and laboratory studies, in which the optical properties of BrC were attributed to specific chromophores and their atmospheric transformations. BBOA represents the primary source of BrC in the atmosphere and therefore molecular-specific analysis of BBOA samples was a focus of many studies. Lin et al.¹³⁵ examined freshly emitted BBOA samples collected during test burns of sawgrass, peat, ponderosa pine, and black spruce. The fuels shared a number of common BrC chromophores, including nitro-aromatics, polycyclic aromatic hydrocarbon derivatives, and polyphenols. However, several biofuel-specific BrC chromophores also were observed. About 50% of light absorption could be

attributed to a limited number of strong BrC chromophores. In a related study, Weggler et al.¹⁴⁴ used thermal desorption and in situ derivatization coupled to 2D GC-TOF-MS analysis for identification of the biomass-type specific BBOA markers. The chemometric tools were used to reduce the data sets and identify the molecular-specific features in the emissions from burning of different biofuels. They observed several important differences between BBOA formed from beech, birch, and spruce: (1) enhancement of small polar compounds in the smoke from beech, (2) efficient formation of methylated naphthalenes and tetra/pentacyclic triterpenoids in birch combustion, and (3) formation of retene and resinic acid derivatives in spruce combustion.

A study of the BBOA samples collected during a national bonfire festival (Lag Ba'Omer in Israel) conducted by Lin et al.^{145,146} showed that a majority of chromophores in the samples were nitroaromatic compounds (Figure 7a,b). These species accounted for 50–80% of the total absorption by BrC, as illustrated in Figure 7c. The results suggested that night time reactions of $\bullet\text{NO}_3$ and N_2O_5 with particles may play a significant role in the formation of nitroaromatic chromophores and their atmospheric transformations. Comparing to the fresh BBOA emission, the atmospheric aging of BBOA smoke in the presence of urban oxidants resulted in a greater structural similarity among individual BrC chromophores. Finally, it was also demonstrated that the aerosol acidity is an important factor contributing to light absorption by BrC. Specifically, ionization of nitrophenols at higher pH results in a red shift in their absorption spectrum. This means that the same BrC compound can become more absorbing when acidic BrC particles are scavenged by less acidic cloud or fog droplets.

Budisulistiorini et al.¹⁴⁷ applied similar methods to the analysis of BBOA emitted by combustion of peat, fern/leaf, and charcoal from Indonesia as well as ambient particulate matter samples collected in Singapore during a haze episode. They identified 41 compounds that can potentially absorb near-UV and visible radiation including oxygenated–conjugated compounds, nitroaromatics, and S-containing compounds. The compounds were shown to make a minor contribution to the aerosol mass but a major contribution to the absorption coefficient. Similar results were also reported by Teich et al.,¹⁴⁸ who studied the molecular composition of BrC chromophores present in water-soluble extracts of aerosols collected at selected locations in Germany and China. In that study, the contribution of nitro-aromatics to the total BrC absorption was found to be 5 times higher than their relative contribution to the total sample mass, indicating that even small amounts of nitro-aromatic chromophores have a disproportionately pronounced effect on the overall light absorption.

Constabile et al.¹⁴⁹ conducted a field study in the Po Valley (one of the most polluted areas in Europe), in which complementary in situ measurements of the aerosol composition by AMS, particle size, light absorption, and scattering were used to understand the relationship between the chemical composition and optical properties of BrC. In that geographic location, the authors observed that the formation of BrC with values of the Angstrom Absorption Exponent at the level of 3.2–5.5 (high wavelength dependence) was correlated with the appearance of the aqueous-phase processed OA and the time periods with high OA-to-black carbon ratios. The later was previously suggested as a basis for practical classification and parametrization of BrC in atmospheric models.¹⁵⁰

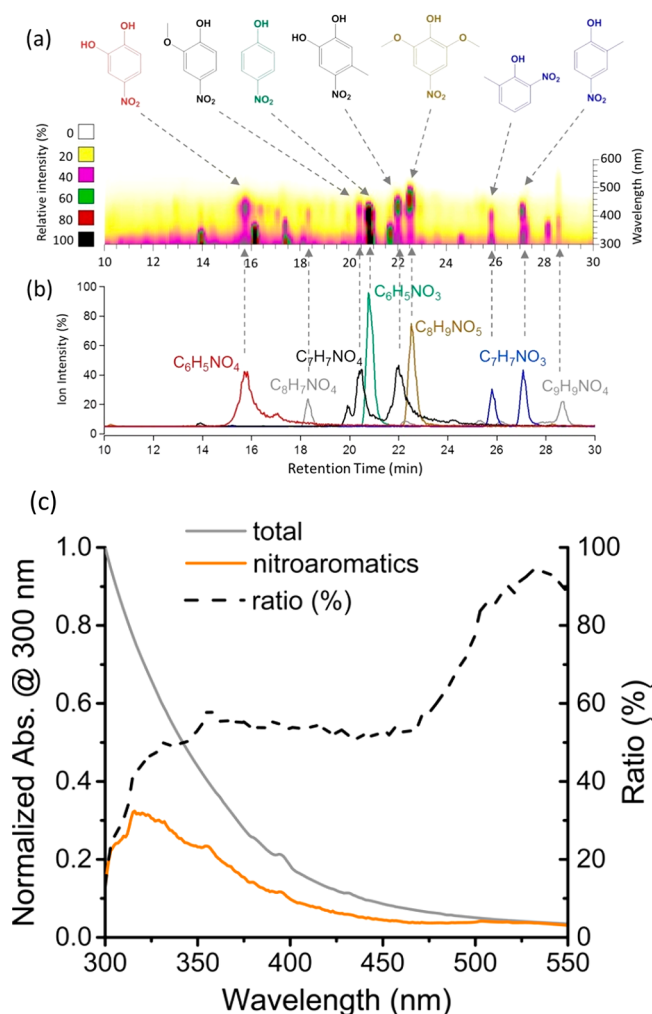


Figure 7. (a) Segments of HPLC-PDA chromatogram and (b) extracted ion MS chromatograms showing the separation of highly absorbing nitro-aromatic chromophores identified in the BBOA sample collected during a bonfire festival at Rehovot, Israel. Reproduced from Broadband optical properties of biomass-burning aerosol and identification of brown carbon chromophores, Bluvshstein, N.; Lin, P.; Flores, J. M.; Segev, L.; Mazar, Y.; Tas, E.; Snider, G.; Weagle, C.; Brown, S. S.; Laskin, A.; Rudich, Y., *J. Geophys. Res. Atmos.* **2017**, *122* (10), 5441–5456 (ref 146). Copyright 2017 Wiley. (c) Total BrC light absorption (gray line), absorption from the identified nitroaromatics (orange line), and the ratio of identified/total absorption (black dash) vs wavelength. Reproduced from Lin, P.; Bluvshstein, N.; Rudich, Y.; Nizkorodov, S.; Laskin, J.; Laskin, A., *Environ. Sci. Technol.* **2017**, *51*, 11561–11570 (ref 145). Copyright 2017 American Chemical Society.

Chen et al.¹⁵¹ used HR-TOF-AMS for the laboratory based correlative analysis of BrC constituents in aerosols samples collected in the urban area of Nagoya, Japan. Aqueous, organic solvent, and solid-phase extractions were performed to distinguish different fractions of organic compounds based on their polarities and solubility. Optical properties of the separated fractions were characterized by UV–vis absorption and excitation–emission matrixes spectroscopy, while chemical composition was analyzed by FT-IR and by HR-AMS. It was found that the intensity of the characteristic excitation–emission components was correlated with the appearance of specific AMS ions and functional groups in FT-IR. This

correlation provides the basis for the classification of BrC chromophores in atmospheric OA.^{151,152}

Unlike the primary BrC emitted in the atmosphere directly from the biomass burning sources, secondary BrC is produced by multiphase atmospheric reactions of originally nonabsorbing organic molecules. Reaction between methyl glyoxal (MG) and ammonium sulfate (AS) is frequently used as a model for secondary BrC formation. Lin et al.⁵⁵ used HPLC-PDA-ESI-HRMS optimized for the efficient separation of the chromophoric compounds to examine the products of this reaction. Aiona et al.¹⁵³ used the same method for analysis of BrC prepared by evaporation of MG + AS solutions instead of slower solution-phase reactions. They showed that both the distribution of chromophores and their relative concentrations were drastically changed in the evaporation experiments, highlighting the dependence of the BrC composition on its formation conditions. The important chromophores contributing to BrC absorption in these mixtures were identified as complex oligomer products containing imidazole and pyrrole rings.

Kampf et al.¹⁵⁴ utilized UHPLC-PDA-ESI-HRMS measurements to study products of reaction between 1,2-, 1,3-, 1,4-, and 1,5- dicarbonyls with AS and glycine. They found that nitrogen heterocycles represent common structural motifs of BrC chromophores formed in such reactions. In particular, reactions of 1,4- and 1,5-dicarbonyls lead to rapid formation of products absorbing at 450 nm. In a related work, Aiona et al.¹⁵⁵ demonstrated that 4-oxopentanal (4-OPA) produced 2-methyl pyrrole (2-MP) in reaction with ammonium sulfate. While 2-MP does not absorb visible radiation, it was shown to further react with 4-OPA eventually forming BrC compounds. Dicarbonyls are common oxidation products of terpenoids and this chemistry is a potentially important pathway to BrC formation.

Secondary BrC also can be produced by the oxidation of aromatic compounds in the presence of NO_x. Lin et al.¹⁵⁶ studied the effect of NO_x on the distribution of chromophores in SOA produced from toluene. The SOA produced under low-NO_x conditions was not light absorbing, whereas SOA material produced at high-NO_x conditions was visibly brown. HPLC-PDA-ESI-HRMS analysis showed that nitrophenols were the primary chromophores in the high-NO_x SOA samples. The specific structural assignments of the chromophores were performed based on the elemental formulas obtained from the accurate mass measurements, complemented with the analysis of standards and quantum mechanical calculations of the proposed structures.

Atmospheric Chemistry at the Air–Water Interface.

Using the ISAT-MS approach highlighted in the methods section, Thomas et al.⁴² examined the reactivity of ozone with oleic acid. Importantly, the authors were able to prove that the ISAT-MS preferentially ionizes surface active species. In the interfacial reaction between ozone and oleic acid, 9-oxononanoic acid was the major product, which also is a major product of the bulk reaction between oleic acid and ozone. Zhang et al.¹⁵⁷ explored the mechanism of oxidation of oleic acid by OH at the air–water interface using field-induced droplet ionization mass spectrometry (FIDI-MS). The kinetics were consistent with a Langmuir–Hinshelwood mechanism. The major primary products corresponded to an addition of a carbonyl or a combination of a carbonyl and hydroxyl groups. Once the C=C bond was oxidized, further oxidation of the saturated carbon chain was observed resulting progressively in

more water-soluble and less surface-active products. The time-resolved capability of FIDI-MS made it possible to directly observe the effect of selective diffusion of the more soluble products of oxidation in the bulk of the droplet. The more soluble products disappeared from the FIDI mass spectra after a short delay following the OH pulse, while the more surface-active products remained.

Other MS-based studies of the chemical processes occurring at the air–water interface have taken advantage of the fact that ions produced from evaporating charged droplets originate predominately from the interfacial layers of the droplets. In 2007, Enami et al.¹⁵⁸ described an approach for studying reactions at a liquid–gas interface using surface-sensitive ESI. In these experiments illustrated in Figure 8a, an aqueous microjet

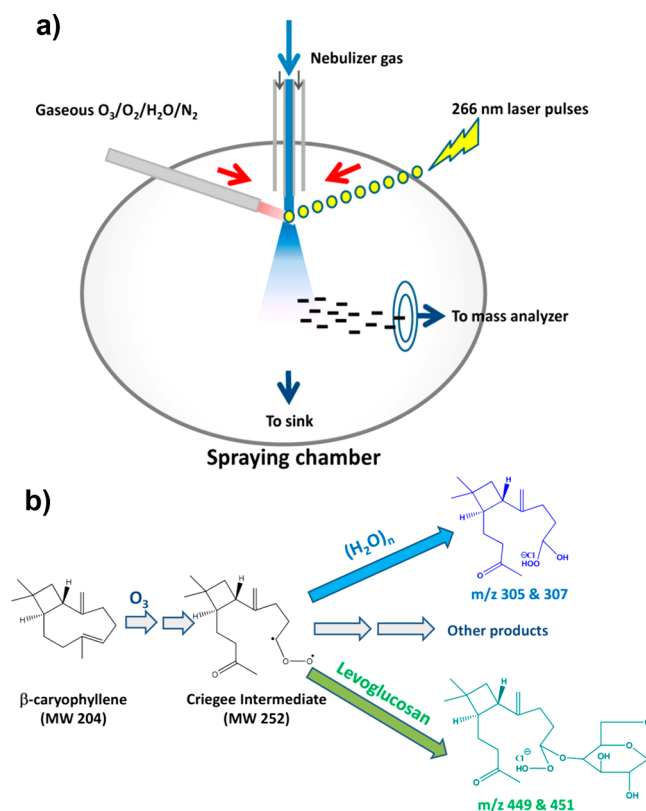


Figure 8. (a) Schematic diagram of the setup for studying reactions of OH at the air–water interface using MS. The same instrument, with the laser pulse omitted, can be used to study reactions of ozone. Reproduced from Enami, S.; Hoffmann, M. R.; Colussi, A. J., *J. Phys. Chem. A* 2014, 118, 4130–4137 (ref 159). Copyright 2014 American Chemical Society. (b) Mechanism of the interfacial reaction between a carbonyl oxide and levoglucosan. The carbonyl oxide is produced by the interfacial reaction of ozone with β-caryophyllene. Reproduced from Enami, S.; Hoffmann, M. R.; Colussi, A. J., *J. Phys. Chem. Lett.* 2017, 8, 3888–3894 (ref 163). Copyright 2017 American Chemical Society.

containing analyte molecules is exposed to a gaseous reagent such as ozone, other reactive gases, or short-lived radical reactants produced by laser flash photolysis.¹⁵⁹ Charged droplets formed when the microjet breaks up (~10–50 μs after being formed) are subsequently transferred to a mass spectrometer inlet and the ions corresponding to reactants and products are directly observed by ESI-MS. This experimental approach has been used in several recent studies to examine

reactions of ozone and various free radicals on aqueous surfaces.

For example, Enami and Colussi¹⁶⁰ showed that carbonyl oxides (also known as Criegee intermediates) produced at the air–water interface of millimolar aqueous solutions of different analytes react more efficiently with dissolved carboxylic acids and alcohols than with water molecules. The competitiveness of the reaction with carboxylic acids and alcohols with respect to reaction with water was found to increase with an increase in the carboxylic acid chain length. In multiple follow-up papers, reactions of carbonyl oxides at the liquid–gas interface were found to effectively consume *cis*-pinonic acid,¹⁶¹ various alcohols,¹⁶² and saccharides, including levoglucosan.¹⁶³ Figure 8b shows the proposed mechanism of reaction between a carbonyl oxide with levoglucosan as well as the competing reaction of this carbonyl oxide with water. In these experiments, the carbonyl oxide was produced by the interfacial reaction of ozone with β -caryophyllene. The fast consumption of levoglucosan at the surface of water is important as it may call into question the common use of levoglucosan as a stable tracer of biomass burning.

MS also has been used to study chemistry at more complex liquid interfaces. Particular attention was given to photosensitized processes occurring at the air–sea interface. Ciuraru et al.¹⁶⁴ observed a large flux of isoprene from irradiated organic films on the ocean surface using Selective Reagent Ionization PTR-TOF-MS with both NO^+ and H_3O^+ as reagents. They suggested that the initial step in the mechanism was hydrogen atom abstraction by an excited photosensitizer (humic acid) from a surfactant (nonanoic acid). However, subsequent steps eventually leading to isoprene are still poorly understood. Hydrogen atom abstraction was confirmed by direct observation of the photosensitized conversion of linear saturated fatty acids into unsaturated gas phase products at the air–water interface.¹⁶⁴ Subsequent reaction of these unsaturated products with gas-phase ozone was shown to produce secondary products including glyoxal¹⁶⁵ and organic aerosol particles.¹⁶⁶ In the latest study in this series, Brüggemann et al.¹⁶⁷ were able to measure emission fluxes for multiple unsaturated and functionalized VOCs from irradiated films of biogenic compounds using a combination of online-APCI-HRMS and PTR-TOF-MS. The fluxes were higher from biofilms containing dead cells than for biofilms containing living cells. The authors concluded that interfacial photochemistry of biogenic surfactants is a major source of abiotic VOCs.

Rapf et al.¹⁶⁸ used ESI-MS to demonstrate that UV irradiation of α -ketoacids at the water–air interface produces a complex mixture of dimeric, trimeric, and larger compounds by radical-driven mechanisms. These reactions can form lipid-like molecules from prebiotic starting materials. Rossignol et al.¹⁶⁹ reported that aqueous solutions covered with just over a monolayer of nonanoic acid produced saturated and unsaturated aldehydes as gas-phase products when irradiated with a 280–320 nm light, even without an intentionally added photosensitizer. This is an unexpected finding given that carboxylic acids are not expected to absorb radiation in this range of wavelengths. The authors attributed the observed reactivity to the formation of the triplet state of nonanoic acid through a weak transition. Further work may be needed to confirm these unusual photochemical reactions in monolayers of surface-active carboxylic acids.

Sui et al.¹⁷⁰ described a novel application of TOF-SIMS method for the in situ sampling of a liquid surface through a

small opening in a microfluidics device. They used an approach called SALVI (for System for Analysis at the Liquid Vacuum Interface) to study photochemical and dark reactions in aqueous solutions of glyoxal and hydrogen peroxide (H_2O_2). Both imaging and depth-profiling of solutions have been demonstrated. SALVI was used for detecting both known and previously unreported aqueous oxidation products of glyoxal, including malonic, succinic, malic, tartaric, formic, and glyoxylic acids, and oligomeric compounds.

Sea Spray Aerosol. A complementary combination of the advanced SPMS and HPLC-ESI-HRMS techniques was used in a series of studies focused on the impact of sea spray aerosol (SSA)^{171–173} on climate. MS was used for characterizing the size and chemical composition of individual SSA particles¹⁷⁴ and relevant algae cells,¹⁷⁵ molecular-level analysis of the organic constituents of SSA,¹⁷⁶ and understanding the effect of SSA composition to their hygroscopic properties.¹⁷⁷ Numerous classes of organic molecules were identified in submicrometer- and supermicrometer fractions of SSA including saturated and unsaturated fatty acids, oxo-fatty acids, saturated hydroxy-fatty acids, mono- and polysaccharides, organosulfates, sulfonates, and other. The distribution of organic species was found to depend strongly on the levels of biological activity in the seawater. Enrichment of shorter-chain fatty acids in the fine fraction of SSA was inferred based on the HPLC-ESI-HRMS data.¹⁷⁶ Selected types of SSA were further characterized using depth-profiling experiments. In these experiments, particles are interrogated by SPMS using a range of desorption and ionization laser pulse energies. The observed change in the particle composition as a function of the laser power extracted from the measured ion intensities was used to describe chemical heterogeneity of individual particles. Depth profiling experiments were performed for atmospheric SSA observed in field studies and model SSA generated in the test facility studies.¹⁷⁴ The results showed heterogeneous core–shell structures of submicrometer-size SSA particles containing a sodium chloride core and a predominately organic shell. SPMS data was used to describe chemical signatures of biological SSA particles (BioSS),¹⁷⁸ which were found to have their ion signatures resembling those observed in terrestrial airborne microbe studies. On the basis of the analysis of the mass spectral features, it was inferred that dry BioSS particles have likely heterogeneous structures, with microbes adhered to sea salt cores. Measurements of optical and hygroscopic properties of SSA indicated that the amount, chemical nature and internal stratification of their organic constituents in SSA have a strong effect on their light scattering ability. This finding indicates that the widely accepted treatment of SSA as sea salt in atmospheric models should be critically reassessed. Gansch et al.¹⁷⁹ used SPMS and electron microscopy to characterize SSA particles observed in Alaska under clean and oil-field (Prudhoe Bay) influenced conditions. They reported substantial influence of the Prudhoe Bay emissions on the composition and internal structures of particles which were found to contain additional anthropogenic organics and soot inclusions characteristic for the air pollution events in that area.

■ SUMMARY AND OUTLOOK

In this review, we presented an overview of the recent advances in the MS instrumentation and methodology applied to a broad range of studies in atmospheric chemistry and highlighted several research directions that benefited from these developments. The examples of MS studies highlighted in this review,

as well as numerous other studies published in the past 3 years, amply demonstrate the power of MS in providing detailed information on the composition and reactivity of atmospheric gases, clusters, particles, and droplets. Substantial progress has been made in the development of approaches for quantitative and sensitive detection of atmospheric gases, collection, ionization, and separation of aerosol compounds for MS analysis, structural characterization of both gaseous and particle-phase aerosol components using IMS-MS, studying reaction kinetics at air–liquid interfaces, chemical analysis and imaging of individual particles, and other research directions. These advances have been used to obtain a detailed understanding of the effect of highly oxidized VOCs on particle nucleation in the atmosphere, mechanisms of chemical aging of OA, factors contributing to the formation and properties of light-absorbing particles, viscous organic particles, and chemistry occurring at the air–water interfaces.

Several important challenges for the application of MS in atmospheric chemistry still remain. We anticipate new developments in the following areas in the next several years:

(i) Development of approaches for quantitative analysis of complex OA samples using ESI and ambient ionization methods. Because OA contains a large number of molecules with ionization efficiencies varying by orders of magnitude, signal suppression during ionization may result in severe discrimination against certain classes of compounds. Furthermore, loss of analyte molecules in the MS inlet and their fragmentation prior to mass analysis are important factors limiting the application of MS for quantitative analysis. As a result, a majority of studies relying on direct infusion of the analyte mixtures are currently limited to qualitative comparisons between different samples. Quantification of compounds in complex mixtures using MS is a challenge that extends well beyond the field of aerosol characterization and is currently being addressed by the scientific community. Substantial improvement of both sampling and ionization will benefit numerous applications focused on complex mixture analysis using MS.

(ii) New experimental methods for field and real-time measurements with performance characteristics comparable to the existing offline analysis techniques will be developed to enable rapid molecular-level characterization of atmospheric aerosols in their native state. Some of these developments will be focused on decreasing the analysis time along with instrument size and cost of the existing offline techniques, which will occur in parallel with substantial improvement in the capabilities of the field-deployable MS instrumentation.

(iii) Development of hyphenated approaches for the simultaneous measurement of the chemical composition and physical properties of aerosols is critically important to understanding chemical aging of OA and its effect on human health, air quality, and climate. For example, methods for HRMS analysis of the chemical composition combined with UV–vis detection of absorption spectra of chromatographically separated organic compounds already exist and are providing a wealth of new information about light-absorbing aerosols. We anticipate the development of multimodal approaches to enable correlation between the chemical composition of atmospheric aerosols with other important properties of aerosol components including toxicity, ROS activity, glass transition temperature, volatility, solubility, photochemical stability, and others.

AUTHOR INFORMATION

Corresponding Author

*E-mail: jlaskin@purdue.edu. Phone: +1-765-494-5464.

ORCID

Julia Laskin: 0000-0002-4533-9644

Alexander Laskin: 0000-0002-7836-8417

Sergey A. Nizkorodov: 0000-0003-0891-0052

Notes

The authors declare no competing financial interest.

Biographies

Julia Laskin received her Master's degree in Physics from the Polytechnical Institute, St. Petersburg, Russia, in 1990 and Ph.D. degree in Physical Chemistry from the Hebrew University of Jerusalem (1998). She was a postdoctoral fellow at the University of Delaware (1998–1999) and PNNL (2000–2002). She was a research scientist at PNNL in 2002–2017. In 2017, she joined the Department of Chemistry at Purdue University as the William F. and Patty J. Miller Professor of Analytical Chemistry. Her research is focused on understanding collisions of complex ions with surfaces, selective surface modification using ion beams, and development of new approaches for chemical analysis of organic aerosols and imaging of biological materials.

Alexander Laskin received his undergraduate degree from the Polytechnical Institute, St. Petersburg, Russia, in 1991 in Physics, and Ph.D. degree in Physical Chemistry from the Hebrew University of Jerusalem, Israel, in 1998. Following postdoctoral research appointments at the University of Delaware, Princeton University, and Pacific Northwest National Laboratory (PNNL), he was a research scientist at PNNL in 2001–2017. In 2017, he joined Purdue University as a Professor of Chemistry. His present and past research interests include physical and analytical chemistry of aerosols, environmental and atmospheric effects of aerosols, chemical imaging and molecular level studies of aerosols, microspectroscopy and high-resolution mass spectrometry of aerosols, combustion-related aerosols, combustion chemistry, and chemical kinetics.

Sergey A. Nizkorodov received his undergraduate degree in Biochemistry from Novosibirsk State University, Russia, in 1993 and graduate degree in Chemical Physics from Basel University, Switzerland, in 1997. After doing his postdoctoral research in chemical kinetics and reaction dynamics at the University of Colorado at Boulder, and in atmospheric chemistry at the California Institute of Technology, he joined the faculty of the Department of Chemistry, University of California, Irvine, in 2002. His current research focus is on chemical reactions occurring in organic particles resulting from interactions of particles with sunlight, reactive oxidizing and reducing trace gases, and water vapor.

ACKNOWLEDGMENTS

The authors gratefully acknowledge funding from the U.S. Department of Commerce and National Oceanic and Atmospheric Administration Climate Program Office's AC4 program, as well as Awards NA16OAR4310101 and NA16OAR4310102, for research support at the time of this manuscript compilation. Additional support for previous and ongoing research projects described in this review has been provided by the U.S. Department of Energy's (DOE) Office of Biological and Environmental Research (BER) through its sponsorship of the William R. Wiley Environmental Molecular Sciences Laboratory (EMSL), DOE-BER Atmospheric System Research program (A.L.); DOE's Office of Basic Energy

Sciences, Division of Chemical Sciences, Geosciences and Biosciences (J.L.); and U.S. National Science Foundation Grants AGS-1227579 and CHE-1337080 (S.A.N.).

REFERENCES

- (1) Shrivastava, M.; Cappa, C. D.; Fan, J. W.; Goldstein, A. H.; Guenther, A. B.; Jimenez, J. L.; Kuang, C.; Laskin, A.; Martin, S. T.; Ng, N. L.; Petaja, T.; Pierce, J. R.; Rasch, P. J.; Roldin, P.; Seinfeld, J. H.; Shilling, J.; Smith, J. N.; Thornton, J. A.; Volkamer, R.; Wang, J.; Worsnop, D. R.; Zaveri, R. A.; Zelenyuk, A.; Zhang, Q. *Rev. Geophys.* **2017**, *55*, 509–559.
- (2) Hallquist, M.; Wenger, J. C.; Baltensperger, U.; Rudich, Y.; Simpson, D.; Claeys, M.; Dommen, J.; Donahue, N. M.; George, C.; Goldstein, A. H.; Hamilton, J. F.; Herrmann, H.; Hoffmann, T.; Iinuma, Y.; Jang, M.; Jenkin, M. E.; Jimenez, J. L.; Kiendler-Scharr, A.; Maenhaut, W.; McFiggans, G.; Mentel, T. F.; Monod, A.; Prevot, A. S. H.; Seinfeld, J. H.; Surratt, J. D.; Szmigielski, R.; Wildt, J. *Atmos. Chem. Phys.* **2009**, *9*, 5155–5236.
- (3) Pöschl, U.; Shiraiwa, M. *Chem. Rev.* **2015**, *115*, 4440–4475.
- (4) Prather, K. A.; Hatch, C. D.; Grassian, V. H. *Annu. Rev. Anal. Chem.* **2008**, *1*, 485–514.
- (5) Zhang, R.; Wang, G.; Guo, S.; Zamora, M. L.; Ying, Q.; Lin, Y.; Wang, W.; Hu, M.; Wang, Y. *Chem. Rev.* **2015**, *115*, 3803–3855.
- (6) Laskin, A.; Laskin, J.; Nizkorodov, S. A. *Chem. Rev.* **2015**, *115*, 4335–4382.
- (7) Nozière, B.; Kalberer, M.; Claeys, M.; Allan, J.; D'Anna, B.; Decesari, S.; Finessi, E.; Glasius, M.; Grgic, I.; Hamilton, J. F.; Hoffmann, T.; Iinuma, Y.; Jaoui, M.; Kahnt, A.; Kampf, C. J.; Kourtchev, I.; Maenhaut, W.; Marsden, N.; Saarikoski, S.; Schnelle-Kreis, J.; Surratt, J. D.; Szidat, S.; Szmigielski, R.; Wisthaler, A. *Chem. Rev.* **2015**, *115*, 3919–3983.
- (8) Moise, T.; Flores, J. M.; Rudich, Y. *Chem. Rev.* **2015**, *115*, 4400–4439.
- (9) Barsanti, K. C.; Kroll, J. H.; Thornton, J. A. *J. Phys. Chem. Lett.* **2017**, *8*, 1503–1511.
- (10) Pratt, K. A.; Prather, K. A. *Mass Spectrom. Rev.* **2012**, *31*, 17–48.
- (11) Pratt, K. A.; Prather, K. A. *Mass Spectrom. Rev.* **2012**, *31*, 1–16.
- (12) Laskin, A.; Laskin, J.; Nizkorodov, S. A. *Environ. Chem.* **2012**, *9*, 163–189.
- (13) Laskin, J.; Laskin, A.; Nizkorodov, S. A. *Int. Rev. Phys. Chem.* **2013**, *32*, 128–170.
- (14) Nozière, B.; Kalberer, M.; Claeys, M.; Allan, J.; D'Anna, B.; Decesari, S.; Finessi, E.; Glasius, M.; Grgić, I.; Hamilton, J. F.; Hoffmann, T.; Iinuma, Y.; Jaoui, M.; Kahnt, A.; Kampf, C. J.; Kourtchev, I.; Maenhaut, W.; Marsden, N.; Saarikoski, S.; Schnelle-Kreis, J.; Surratt, J. D.; Szidat, S.; Szmigielski, R.; Wisthaler, A. *Chem. Rev.* **2015**, *115*, 3919–3983.
- (15) Parshintsev, J.; Hyotylainen, T. *Anal. Bioanal. Chem.* **2015**, *407*, 5877–5897.
- (16) Hayes, P. L. *Analyst* **2017**, *142*, 687–690.
- (17) Yuan, B.; Koss, A. R.; Warneke, C.; Coggon, M.; Sekimoto, K.; de Gouw, J. A. *Chem. Rev.* **2017**, *117*, 13187–13229.
- (18) Perraud, V.; Meinardi, S.; Blake, D. R.; Finlayson-Pitts, B. J. *Atmos. Meas. Tech.* **2016**, *9*, 1325–1340.
- (19) Barreira, L. M. F.; Xue, Y.; Dupont, G.; Parshintsev, J.; Hartonen, K.; Jussila, M.; Kulmala, M.; Riekkola, M. L. *Atmos. Meas. Tech.* **2016**, *9*, 3661–3671.
- (20) Dhummakupt, E. S.; Mach, P. M.; Carmany, D.; Demond, P. S.; Moran, T. S.; Connell, T.; Wylie, H. S.; Manicke, N. E.; Nilles, J. M.; Glaros, T. *Anal. Chem.* **2017**, *89*, 10866–10872.
- (21) Lopez-Hilfiker, F. D.; Iyer, S.; Mohr, C.; Lee, B. H.; D'Ambro, E. L.; Kurten, T.; Thornton, J. A. *Atmos. Meas. Tech.* **2016**, *9*, 1505–1512.
- (22) Iyer, S.; Lopez-Hilfiker, F.; Lee, B. H.; Thornton, J. A.; Kurten, T. *J. Phys. Chem. A* **2016**, *120*, 576–587.
- (23) Brophy, P.; Farmer, D. K. *Atmos. Meas. Tech.* **2016**, *9*, 3969–3986.
- (24) Yuan, B.; Koss, A.; Warneke, C.; Gilman, J. B.; Lerner, B. M.; Stark, H.; de Gouw, J. A. *Atmos. Meas. Tech.* **2016**, *9*, 2735–2752.
- (25) Lopez-Hilfiker, F. D.; Mohr, C.; Ehn, M.; Rubach, F.; Kleist, E.; Wildt, J.; Mentel, T. F.; Carrasquillo, A. J.; Daumit, K. E.; Hunter, J. F.; Kroll, J. H.; Worsnop, D. R.; Thornton, J. A. *Atmos. Chem. Phys.* **2015**, *15*, 7765–7776.
- (26) Simon, M.; Heinritzi, M.; Herzog, S.; Leiminger, M.; Bianchi, F.; Praplan, A.; Dommen, J.; Curtius, J.; Kurten, A. *Atmos. Meas. Tech.* **2016**, *9*, 2135–2145.
- (27) Kim, M. J.; Zoerb, M. C.; Campbell, N. R.; Zimmermann, K. J.; Blomquist, B. W.; Huebert, B. J.; Bertram, T. H. *Atmos. Meas. Tech.* **2016**, *9*, 1473–1484.
- (28) Oberreit, D.; Rawat, V. K.; Larriba-Andaluz, C.; Ouyang, H.; McMurry, P. H.; Hogan, C. J. *J. Chem. Phys.* **2015**, *143*, 104204.
- (29) Li, C. X.; Hogan, C. J., Jr. *Aerosol Sci. Technol.* **2017**, *51*, 653–664.
- (30) Thomas, J. M.; He, S. Q.; Larriba-Andaluz, C.; DePalma, J. W.; Johnston, M. V.; Hogan, C. J., Jr. *Phys. Chem. Chem. Phys.* **2016**, *18*, 22962–22972.
- (31) Krechmer, J. E.; Groessl, M.; Zhang, X.; Junninen, H.; Massoli, P.; Lambe, A. T.; Kimmel, J. R.; Cubison, M. J.; Graf, S.; Lin, Y. H.; Budisulistiorini, S. H.; Zhang, H. F.; Surratt, J. D.; Knochenmuss, R.; Jayne, J. T.; Worsnop, D. R.; Jimenez, J. L.; Canagaratna, M. R. *Atmos. Meas. Tech.* **2016**, *9*, 3245–3262.
- (32) Zhang, X.; Krechmer, J. E.; Groessl, M.; Xu, W.; Graf, S.; Cubison, M.; Jayne, J. T.; Jimenez, J. L.; Worsnop, D. R.; Canagaratna, M. R. *Atmos. Chem. Phys.* **2016**, *16*, 12945–12959.
- (33) Horan, A. J.; Apsokardu, M. J.; Johnston, M. V. *Anal. Chem.* **2017**, *89*, 1059–1062.
- (34) Trimpin, S.; Wang, B. X.; Inutan, E. D.; Li, J.; Lietz, C. B.; Harron, A.; Pagnotti, V. S.; Sardelis, D.; McEwen, C. N. *J. Am. Soc. Mass Spectrom.* **2012**, *23*, 1644–1660.
- (35) Zhai, Y. B.; Jiang, T.; Huang, G. Y.; Wei, Y. Z.; Xu, W. *Analyst* **2016**, *141*, 5404–5411.
- (36) Forbes, T. P.; Staymates, M. *Anal. Chim. Acta* **2017**, *957*, 20–28.
- (37) Zhao, Y.; Fairhurst, M. C.; Wingen, L. M.; Perraud, V.; Ezell, M. J.; Finlayson-Pitts, B. J. *Atmos. Meas. Tech.* **2017**, *10*, 1373–1386.
- (38) Kumbhani, S. R.; Wingen, L. M.; Perraud, V.; Finlayson-Pitts, B. J. *Rapid Commun. Mass Spectrom.* **2017**, *31*, 1659–1668.
- (39) Bruggemann, M.; Karu, E.; Hoffmann, T. *J. Mass Spectrom.* **2016**, *51*, 141–149.
- (40) Smith, J. N.; Moore, K. F.; McMurry, P. H.; Eisele, F. L. *Aerosol Sci. Technol.* **2004**, *38*, 100–110.
- (41) He, S.; Li, L.; Duan, H.; Naqwi, A.; Hogan, C. J. *Anal. Chem.* **2015**, *87*, 6752–6760.
- (42) Thomas, D. A.; Wang, L. T.; Goh, B.; Kim, E. S.; Beauchamp, J. L. *Anal. Chem.* **2015**, *87*, 3336–3344.
- (43) Ahmed, M.; Guo, X.; Zhao, X.-M. *Microchem. J.* **2017**, *130*, 400–411.
- (44) Cochran, R. E.; Smoliakova, I. P.; Kubatova, A. *Int. J. Mass Spectrom.* **2016**, *397*, 6–17.
- (45) Parshintsev, J.; Vaikkinen, A.; Lipponen, K.; Vrkoslav, V.; Cvačka, J.; Kostianen, R.; Kotiaho, T.; Hartonen, K.; Riekkola, M.-L.; Kauppila, T. J. *Rapid Commun. Mass Spectrom.* **2015**, *29*, 1233–1241.
- (46) Mologousi, A. I.; Bakeas, E. B. *Anal. Methods* **2016**, *8*, 4047–4055.
- (47) Rodigast, M.; Mutzel, A.; Iinuma, Y.; Haferkorn, S.; Herrmann, H. *Atmos. Meas. Tech.* **2015**, *8*, 2409–2416.
- (48) Yu, R.; Duan, L.; Jiang, J. K.; Hao, J. M. *J. Environ. Sci.* **2017**, *53*, 313–321.
- (49) Alam, M. S.; Harrison, R. M. *Chem. Sci.* **2016**, *7*, 3968–3977.
- (50) Martinez, R. E.; Williams, B. J.; Zhang, Y. P.; Hagan, D.; Walker, M.; Kreisberg, N. M.; Hering, S. V.; Hohaus, T.; Jayne, J. T.; Worsnop, D. R. *Aerosol Sci. Technol.* **2016**, *50*, 255–271.
- (51) Alam, M. S.; Stark, C.; Harrison, R. M. *Anal. Chem.* **2016**, *88*, 4211–4220.
- (52) Alam, M. S.; Zeraati-Rezaei, S.; Stark, C. P.; Liang, Z.; Xu, H.; Harrison, R. M. *Faraday Discuss.* **2016**, *189*, 69–84.

- (53) Worton, D. R.; Decker, M.; Isaacman-VanWertz, G.; Chan, A. W. H.; Wilson, K. R.; Goldstein, A. H. *Analyst* **2017**, *142*, 2395–2403.
- (54) Ranney, A. P.; Ziemann, P. J. *Aerosol Sci. Technol.* **2017**, *51*, 342–353.
- (55) Lin, P.; Laskin, J.; Nizkorodov, S. A.; Laskin, A. *Environ. Sci. Technol.* **2015**, *49*, 14257–14266.
- (56) Matejcek, D.; Vasickova, J. *J. Sep. Sci.* **2016**, *39*, 4748–4755.
- (57) Després, V.; Huffman, J. A.; Burrows, S. M.; Hoose, C.; Safatov, A.; Buryak, G.; Fröhlich-Nowoisky, J.; Elbert, W.; Andreae, M.; Pöschl, U.; Jaenicke, R. *Tellus, Ser. B* **2012**, *64*, 15598.
- (58) Fröhlich-Nowoisky, J.; Kampf, C. J.; Weber, B.; Huffman, J. A.; Pohlker, C.; Andreae, M. O.; Lang-Yona, N.; Burrows, S. M.; Gunthe, S. S.; Elbert, W.; Su, H.; Hoor, P.; Thines, E.; Hoffmann, T.; Despres, V. R.; Poschl, U. *Atmos. Res.* **2016**, *182*, 346–376.
- (59) Liu, F. B.; Lai, S. C.; Reinmuth-Selzle, K.; Scheel, J. F.; Fröhlich-Nowoisky, J.; Despres, V.; Hoffmann, T.; Poschl, U.; Kampf, C. J. *Anal. Bioanal. Chem.* **2016**, *408*, 6337–6348.
- (60) Zelenyuk, A.; Imre, D.; Wilson, J.; Zhang, Z.; Wang, J.; Mueller, K. J. *Am. Soc. Mass Spectrom.* **2015**, *26*, 257–270.
- (61) Reitz, P.; Zorn, S. R.; Trimborn, S. H.; Trimborn, A. M. *J. Aerosol Sci.* **2016**, *98*, 1–14.
- (62) Passig, J.; Schade, J.; Oster, M.; Fuchs, M.; Ehlert, S.; Jäger, C.; Sklorz, M.; Zimmermann, R. *Anal. Chem.* **2017**, *89*, 6341–6345.
- (63) Alexander, J. M.; Bell, D. M.; Imre, D.; Kleiber, P. D.; Grassian, V. H.; Zelenyuk, A. *Aerosol Sci. Technol.* **2016**, *50*, 870–879.
- (64) Marsden, N.; Flynn, M. J.; Taylor, J.; Allan, J. D.; Coe, H. *Atmos. Meas. Tech.* **2016**, *9*, 6051–6068.
- (65) Gemayel, R.; Hellebust, S.; Temime-Roussel, B.; Hayeck, N.; Van Elteren, J. T.; Wortham, H.; Gligorovski, S. *Atmos. Meas. Tech.* **2016**, *9*, 1947–1959.
- (66) Wolf, R.; Slowik, J. G.; Schaupp, C.; Amato, P.; Saathoff, H.; Möhler, O.; Prévôt, A. S. H.; Baltensperger, U. *J. Mass Spectrom.* **2015**, *50*, 662–671.
- (67) Sultana, C. M.; Cornwell, G. C.; Rodriguez, P.; Prather, K. A. *Atmos. Meas. Tech.* **2017**, *10*, 1323–1334.
- (68) Li, K. X.; Sinha, B.; Hoppe, P. *Anal. Chem.* **2016**, *88*, 3281–3288.
- (69) Li, K. X.; Sinha, B.; Hoppe, P. *J. Vac. Sci. Technol., B: Nanotechnol. Microelectron.: Mater., Process., Meas., Phenom.* **2016**, *34*, 030601.
- (70) DeCarlo, P. F.; Kimmel, J. R.; Trimborn, A.; Northway, M. J.; Jayne, J. T.; Aiken, A. C.; Gonin, M.; Fuhrer, K.; Horvath, T.; Docherty, K. S.; Worsnop, D. R.; Jimenez, J. L. *Anal. Chem.* **2006**, *78*, 8281–8289.
- (71) Canagaratna, M. R.; Massoli, P.; Browne, E. C.; Franklin, J. P.; Wilson, K. R.; Onasch, T. B.; Kirchstetter, T. W.; Fortner, E. C.; Kolb, C. E.; Jayne, J. T.; Kroll, J. H.; Worsnop, D. R. *J. Phys. Chem. A* **2015**, *119*, 4589–4599.
- (72) Kenseth, C. M.; Petrucci, G. A. *Aerosol Sci. Technol.* **2016**, *50*, 790–801.
- (73) Jokinen, T.; Berndt, T.; Makkonen, R.; Kerminen, V.-M.; Junninen, H.; Paasonen, P.; Stratmann, F.; Herrmann, H.; Guenther, A. B.; Worsnop, D. R.; Kulmala, M.; Ehn, M.; Sipilä, M. *Proc. Natl. Acad. Sci. U. S. A.* **2015**, *112*, 7123–7128.
- (74) Berndt, T.; Herrmann, H.; Kurtén, T. *J. Am. Chem. Soc.* **2017**, *139*, 13387–13392.
- (75) Richters, S.; Herrmann, H.; Berndt, T. *Atmos. Chem. Phys.* **2016**, *16*, 9831–9845.
- (76) Richters, S.; Herrmann, H.; Berndt, T. *Environ. Sci. Technol.* **2016**, *50*, 2354–2362.
- (77) Mentel, T. F.; Springer, M.; Ehn, M.; Kleist, E.; Pullinen, I.; Kurtén, T.; Rissanen, M.; Wahner, A.; Wildt, J. *Atmos. Chem. Phys.* **2015**, *15*, 6745–6765.
- (78) Berndt, T.; Herrmann, H.; Sipilä, M.; Kulmala, M. *J. Phys. Chem. A* **2016**, *120*, 10150–10159.
- (79) Berndt, T.; Richters, S.; Jokinen, T.; Hyttinen, N.; Kurtén, T.; Otkjær, R. V.; Kjaergaard, H. G.; Stratmann, F.; Herrmann, H.; Sipilä, M.; Kulmala, M.; Ehn, M. *Nat. Commun.* **2016**, *7*, 13677.
- (80) Wang, S. N.; Wu, R. R.; Berndt, T.; Ehn, M.; Wang, L. M. *Environ. Sci. Technol.* **2017**, *51*, 8442–8449.
- (81) Zhang, X.; Lambe, A. T.; Upshur, M. A.; Brooks, W. A.; Gray Bé, A.; Thomson, R. J.; Geiger, F. M.; Surratt, J. D.; Zhang, Z.; Gold, A.; Graf, S.; Cubison, M. J.; Groessl, M.; Jayne, J. T.; Worsnop, D. R.; Canagaratna, M. R. *Environ. Sci. Technol.* **2017**, *51*, 5932–5940.
- (82) Mutzel, A.; Poulain, L.; Berndt, T.; Iinuma, Y.; Rodigast, M.; Böge, O.; Richters, S.; Spindler, G.; Sipilä, M.; Jokinen, T.; Kulmala, M.; Herrmann, H. *Environ. Sci. Technol.* **2015**, *49*, 7754–7761.
- (83) Krapf, M.; El Haddad, I.; Bruns, E. A.; Molteni, U.; Daellenbach, K. R.; Prévôt, A. S. H.; Baltensperger, U.; Dommen, J. *Chem.* **2016**, *1*, 603–616.
- (84) Dunne, E. M.; Gordon, H.; Kurten, A.; Almeida, J.; Duplissy, J.; Williamson, C.; Ortega, I. K.; Pringle, K. J.; Adamov, A.; Baltensperger, U.; Barmet, P.; Benduhn, F.; Bianchi, F.; Breitenlechner, M.; Clarke, A.; Curtius, J.; Dommen, J.; Donahue, N. M.; Ehrhart, S.; Flagan, R. C.; Franchin, A.; Guida, R.; Hakala, J.; Hansel, A.; Heinritzi, M.; Jokinen, T.; Kangasluoma, J.; Kirkby, J.; Kulmala, M.; Kupc, A.; Lawler, M. J.; Lehtipalo, K.; Makhmutov, V.; Mann, G.; Mathot, S.; Merikanto, J.; Miettinen, P.; Nenes, A.; Onnela, A.; Rap, A.; Reddington, C. L. S.; Riccobono, F.; Richards, N. A. D.; Rissanen, M. P.; Rondo, L.; Sarnela, N.; Schobesberger, S.; Sengupta, K.; Simon, M.; Sipilä, M.; Smith, J. N.; Stozhkov, Y.; Tome, A.; Trostl, J.; Wagner, P. E.; Wimmer, D.; Winkler, P. M.; Worsnop, D. R.; Carslaw, K. S. *Science* **2016**, *354*, 1119–1124.
- (85) Kirkby, J.; Duplissy, J.; Sengupta, K.; Frege, C.; Gordon, H.; Williamson, C.; Heinritzi, M.; Simon, M.; Yan, C.; Almeida, J.; Tröstl, J.; Nieminen, T.; Ortega, I. K.; Wagner, R.; Adamov, A.; Amorim, A.; Bernhammer, A.-K.; Bianchi, F.; Breitenlechner, M.; Brilke, S.; Chen, X.; Craven, J.; Dias, A.; Ehrhart, S.; Flagan, R. C.; Franchin, A.; Fuchs, C.; Guida, R.; Hakala, J.; Hoyle, C. R.; Jokinen, T.; Junninen, H.; Kangasluoma, J.; Kim, J.; Krapf, M.; Kürten, A.; Laaksonen, A.; Lehtipalo, K.; Makhmutov, V.; Mathot, S.; Molteni, U.; Onnela, A.; Peräkylä, O.; Piel, F.; Petäjä, T.; Praplan, A. P.; Pringle, K.; Rap, A.; Richards, N. A. D.; Riipinen, I.; Rissanen, M. P.; Rondo, L.; Sarnela, N.; Schobesberger, S.; Scott, C. E.; Seinfeld, J. H.; Sipilä, M.; Steiner, G.; Stozhkov, Y.; Stratmann, F.; Tomé, A.; Virtanen, A.; Vogel, A. L.; Wagner, A. C.; Wagner, P. E.; Weingartner, E.; Wimmer, D.; Winkler, P. M.; Ye, P.; Zhang, X.; Hansel, A.; Dommen, J.; Donahue, N. M.; Worsnop, D. R.; Baltensperger, U.; Kulmala, M.; Carslaw, K. S.; Curtius, J. *Nature* **2016**, *533*, 521–526.
- (86) Tröstl, J.; Chuang, W. K.; Gordon, H.; Heinritzi, M.; Yan, C.; Molteni, U.; Ahlm, L.; Frege, C.; Bianchi, F.; Wagner, R.; Simon, M.; Lehtipalo, K.; Williamson, C.; Craven, J. S.; Duplissy, J.; Adamov, A.; Almeida, J.; Bernhammer, A.-K.; Breitenlechner, M.; Brilke, S.; Dias, A.; Ehrhart, S.; Flagan, R. C.; Franchin, A.; Fuchs, C.; Guida, R.; Gysel, M.; Hansel, A.; Hoyle, C. R.; Jokinen, T.; Junninen, H.; Kangasluoma, J.; Keskinen, H.; Kim, J.; Krapf, M.; Kürten, A.; Laaksonen, A.; Lawler, M.; Leiminger, M.; Mathot, S.; Möhler, O.; Nieminen, T.; Onnela, A.; Petäjä, T.; Piel, F. M.; Miettinen, P.; Rissanen, M. P.; Rondo, L.; Sarnela, N.; Schobesberger, S.; Sengupta, K.; Sipilä, M.; Smith, J. N.; Steiner, G.; Tomé, A.; Virtanen, A.; Wagner, A. C.; Weingartner, E.; Wimmer, D.; Winkler, P. M.; Ye, P.; Carslaw, K. S.; Curtius, J.; Dommen, J.; Kirkby, J.; Kulmala, M.; Riipinen, I.; Worsnop, D. R.; Donahue, N. M.; Baltensperger, U. *Nature* **2016**, *533*, 527–531.
- (87) Bianchi, F.; Tröstl, J.; Junninen, H.; Frege, C.; Henne, S.; Hoyle, C. R.; Molteni, U.; Herrmann, E.; Adamov, A.; Bukowiecki, N.; Chen, X.; Duplissy, J.; Gysel, M.; Hutterli, M.; Kangasluoma, J.; Kontkanen, J.; Kürten, A.; Manninen, H. E.; Münch, S.; Peräkylä, O.; Petäjä, T.; Rondo, L.; Williamson, C.; Weingartner, E.; Curtius, J.; Worsnop, D. R.; Kulmala, M.; Dommen, J.; Baltensperger, U. *Science* **2016**, *352*, 1109–1112.
- (88) Mohr, C.; Lopez-Hilfiker, F. D.; Yli-Juuti, T.; Heitto, A.; Lutz, A.; Hallquist, M.; D'Ambro, E. L.; Rissanen, M. P.; Hao, L. Q.; Schobesberger, S.; Kulmala, M.; Mauldin, R. L.; Makkonen, U.; Sipilä, M.; Petaja, T.; Thornton, J. A. *Geophys. Res. Lett.* **2017**, *44*, 2958–2966.
- (89) Vogel, A. L.; Schneider, J.; Müller-Tautges, C.; Klimach, T.; Hoffmann, T. *Environ. Sci. Technol.* **2016**, *50*, 10814–10822.

- (90) Lehtipalo, K.; Rondo, L.; Kontkanen, J.; Schobesberger, S.; Jokinen, T.; Sarnela, N.; Kurten, A.; Ehrhart, S.; Franchin, A.; Nieminen, T.; Riccobono, F.; Sipila, M.; Yli-Juuti, T.; Duplissy, J.; Adamov, A.; Ahlm, L.; Almeida, J.; Amorim, A.; Bianchi, F.; Breitenlechner, M.; Dommen, J.; Downard, A. J.; Dunne, E. M.; Flagan, R. C.; Guida, R.; Hakala, J.; Hansel, A.; Jud, W.; Kangasluoma, J.; Kerminen, V. M.; Keskinen, H.; Kim, J.; Kirkby, J.; Kupc, A.; Kupiainen-Maatta, O.; Laaksonen, A.; Lawler, M. J.; Leiminger, M.; Mathot, S.; Olenius, T.; Ortega, I. K.; Onnela, A.; Petaja, T.; Praplan, A.; Rissanen, M. P.; Ruuskanen, T.; Santos, F. D.; Schallhart, S.; Schnitzhofer, R.; Simon, M.; Smith, J. N.; Trostl, J.; Tsagkogeorgas, G.; Tome, A.; Vaattovaara, P.; Vehkamaki, H.; Virtala, A. E.; Wagner, P. E.; Williamson, C.; Wimmer, D.; Winkler, P. M.; Virtanen, A.; Donahue, N. M.; Carslaw, K. S.; Baltensperger, U.; Riipinen, I.; Curtius, J.; Worsnop, D. R.; Kulmala, M. *Nat. Commun.* **2016**, *7*, 9.
- (91) Lawler, M. J.; Winkler, P. M.; Kim, J.; Ahlm, L.; Trostl, J.; Praplan, A. P.; Schobesberger, S.; Kurten, A.; Kirkby, J.; Bianchi, F.; Duplissy, J.; Hansel, A.; Jokinen, T.; Keskinen, H.; Lehtipalo, K.; Leiminger, M.; Petaja, T.; Rissanen, M.; Rondo, L.; Simon, M.; Sipila, M.; Williamson, C.; Wimmer, D.; Riipinen, I.; Virtanen, A.; Smith, J. N. *Atmos. Chem. Phys.* **2016**, *16*, 13601–13618.
- (92) Duporte, G.; Parshintsev, J.; Barreira, L. M. F.; Hartonen, K.; Kulmala, M.; Riekkola, M. L. *Environ. Sci. Technol.* **2016**, *50*, 4693–4700.
- (93) Duporte, G.; Riva, M.; Parshintsev, J.; Heikkinen, E.; Barreira, L. M. F.; Mylly, N.; Heikkinen, L.; Hartonen, K.; Kulmala, M.; Ehn, M.; Riekkola, M. L. *Environ. Sci. Technol.* **2017**, *51*, S602–S610.
- (94) Rindelaub, J. D.; Wiley, J. S.; Cooper, B. R.; Shepson, P. B. *Rapid Commun. Mass Spectrom.* **2016**, *30*, 1627–1638.
- (95) Lee, B. H.; Mohr, C.; Lopez-Hilfiker, F. D.; Lutz, A.; Hallquist, M.; Lee, L.; Romer, P.; Cohen, R. C.; Iyer, S.; Kurten, T.; Hu, W. W.; Day, D. A.; Campuzano-Jost, P.; Jimenez, J. L.; Xu, L.; Ng, N. L.; Guo, H. Y.; Weber, R. J.; Wild, R. J.; Brown, S. S.; Koss, A.; de Gouw, J.; Olson, K.; Goldstein, A. H.; Seco, R.; Kim, S.; McAvey, K.; Shepson, P. B.; Starn, T.; Baumann, K.; Edgerton, E. S.; Liu, J. M.; Shilling, J. E.; Miller, D. O.; Brune, W.; Schobesberger, S.; D'Ambro, E. L.; Thornton, J. A. *Proc. Natl. Acad. Sci. U. S. A.* **2016**, *113*, 1516–1521.
- (96) Riva, M.; Bell, D. M.; Hansen, A. M. K.; Drozd, G. T.; Zhang, Z. F.; Gold, A.; Imre, D.; Surratt, J. D.; Glasius, M.; Zelenyuk, A. *Environ. Sci. Technol.* **2016**, *50*, 5580–5588.
- (97) Gallimore, P. J.; Griffiths, P. T.; Pope, F. D.; Reid, J. P.; Kalberer, M. *J. Geophys. Res. Atmos.* **2017**, *122*, 4364–4377.
- (98) Gallimore, P. J.; Mahon, B. M.; Wragg, F. P. H.; Fuller, S. J.; Giorio, C.; Kourtchev, I.; Kalberer, M. *Atmos. Chem. Phys.* **2017**, *17*, 9853–9868.
- (99) Kourtchev, I.; Giorio, C.; Manninen, A.; Wilson, E.; Mahon, B.; Aalto, J.; Kajos, M.; Venables, D.; Ruuskanen, T.; Levula, J.; Lopenon, M.; Connors, S.; Harris, N.; Zhao, D. F.; Kiendler-Scharr, A.; Mentel, T.; Rudich, Y.; Hallquist, M.; Doussin, J. F.; Maenhaut, W.; Back, J.; Petaja, T.; Wenger, J.; Kulmala, M.; Kalberer, M. *Sci. Rep.* **2016**, *6*, 9.
- (100) Tong, H. J.; Kourtchev, I.; Pant, P.; Keyte, I. J.; O'Connor, I. P.; Wenger, J. C.; Pope, F. D.; Harrison, R. M.; Kalberer, M. *Faraday Discuss.* **2016**, *189*, 51–68.
- (101) Willoughby, A. S.; Wozniak, A. S.; Hatcher, P. G. *Atmosphere* **2016**, *7*, 79.
- (102) Blair, S. L.; MacMillan, A. C.; Drozd, G. T.; Goldstein, A. H.; Chu, R. K.; Pasa-Tolic, L.; Shaw, J. B.; Tolic, N.; Lin, P.; Laskin, J.; Laskin, A.; Nizkorodov, S. A. *Environ. Sci. Technol.* **2017**, *51*, 119–127.
- (103) Duporte, G.; Flaud, P. M.; Geneste, E.; Augagneur, S.; Pangui, E.; Lamkaddam, H.; Gratién, A.; Doussin, J. F.; Budzinski, H.; Villenave, E.; Perraudin, E. *J. Phys. Chem. A* **2016**, *120*, 7909–7923.
- (104) Riva, M.; Barbosa, T. D.; Lin, Y. H.; Stone, E. A.; Gold, A.; Surratt, J. D. *Atmos. Chem. Phys.* **2016**, *16*, 11001–11018.
- (105) Barbosa, T. S.; Riva, M.; Chen, Y. Z.; da Silva, C. M.; Azevedo, J. C. S.; Zhang, Z.; Gold, A.; Arbilla, G.; Bauerfeldt, G. F.; Surratt, J. D. *Atmos. Environ.* **2017**, *162*, 141–151.
- (106) Bruggemann, M.; Poulain, L.; Held, A.; Stelzer, T.; Zuth, C.; Richters, S.; Mutzel, A.; van Pinxteren, D.; Iinuma, Y.; Katkevica, S.; Rabe, R.; Herrmann, H.; Hoffmann, T. *Atmos. Chem. Phys.* **2017**, *17*, 1453–1469.
- (107) Vogel, A. L.; Schneider, J.; Müller-Tautges, C.; Phillips, G. J.; Pohlker, M. L.; Rose, D.; Zuth, C.; Makkonen, U.; Hakola, H.; Crowley, J. N.; Andreae, M. O.; Poschl, U.; Hoffmann, T. *Environ. Sci. Technol.* **2016**, *50*, 10823–10832.
- (108) Ervens, B.; Turpin, B. J.; Weber, R. J. *Atmos. Chem. Phys.* **2011**, *11*, 11069–11102.
- (109) Sareen, N.; Carlton, A. G.; Surratt, J. D.; Gold, A.; Lee, B.; Lopez-Hilfiker, F. D.; Mohr, C.; Thornton, J. A.; Zhang, Z.; Lim, Y. B.; Turpin, B. J. *Atmos. Chem. Phys.* **2016**, *16*, 14409–14420.
- (110) Sullivan, A. P.; Hodas, N.; Turpin, B. J.; Skog, K.; Keutsch, F. N.; Gilardoni, S.; Paglione, M.; Rinaldi, M.; Decesari, S.; Facchini, M. C.; Poulain, L.; Herrmann, H.; Wiedensohler, A.; Nemitz, E.; Twigg, M. M.; Collett, J. L., Jr. *Atmos. Chem. Phys.* **2016**, *16*, 8095–8108.
- (111) Gilardoni, S.; Massoli, P.; Paglione, M.; Giulianelli, L.; Carbone, C.; Rinaldi, M.; Decesari, S.; Sandrini, S.; Costabile, F.; Gobbi, G. P.; Pietrogrande, M. C.; Visentin, M.; Scotto, F.; Fuzzi, S.; Facchini, M. C. *Proc. Natl. Acad. Sci. U. S. A.* **2016**, *113*, 10013–10018.
- (112) Faust, J. A.; Wong, J. P. S.; Lee, A. K. Y.; Abbatt, J. P. D. *Environ. Sci. Technol.* **2017**, *51*, 1405–1413.
- (113) Lim, Y. B.; Kim, H.; Kim, J. Y.; Turpin, B. J. *Atmos. Chem. Phys.* **2016**, *16*, 12631–12647.
- (114) Thomas, D. A.; Coggon, M. M.; Lignell, H.; Schilling, K. A.; Zhang, X.; Schwantes, R. H.; Flagan, R. C.; Seinfeld, J. H.; Beauchamp, J. L. *Environ. Sci. Technol.* **2016**, *50*, 12241–12249.
- (115) Renard, P.; Tlili, S.; Ravier, S.; Quivet, E.; Monod, A. *Atmos. Environ.* **2016**, *130*, 153–162.
- (116) Eugene, A. J.; Xia, S.-S.; Guzman, M. I. *J. Phys. Chem. A* **2016**, *120*, 3817–3826.
- (117) Eugene, A. J.; Guzman, M. I. *J. Phys. Chem. A* **2017**, *121*, 2924–2935.
- (118) Rapf, R. J.; Perkins, R. J.; Carpenter, B. K.; Vaida, V. *J. Phys. Chem. A* **2017**, *121*, 4272–4282.
- (119) Lim, Y. B.; Turpin, B. J. *Atmos. Chem. Phys.* **2015**, *15*, 12867–12877.
- (120) Yu, L.; Smith, J.; Laskin, A.; George, K. M.; Anastasio, C.; Laskin, J.; Dillner, A. M.; Zhang, Q. *Atmos. Chem. Phys.* **2016**, *16*, 4511–4527.
- (121) Aljawhary, D.; Zhao, R.; Lee, A. K. Y.; Wang, C.; Abbatt, J. P. D. *J. Phys. Chem. A* **2016**, *120*, 1395–1407.
- (122) Zhao, R.; Aljawhary, D.; Lee, A. K. Y.; Abbatt, J. P. D. *Environ. Sci. Technol. Lett.* **2017**, *4*, 205–210.
- (123) Romonosky, D. E.; Laskin, A.; Laskin, J.; Nizkorodov, S. A. *J. Phys. Chem. A* **2015**, *119*, 2594–2606.
- (124) Romonosky, D. E.; Li, Y.; Shiraiwa, M.; Laskin, A.; Laskin, J.; Nizkorodov, S. A. *J. Phys. Chem. A* **2017**, *121*, 1298–1309.
- (125) Tong, H.; Arangio, A. M.; Lakey, P. S. J.; Berkemeier, T.; Liu, F.; Kampf, C. J.; Brune, W. H.; Pöschl, U.; Shiraiwa, M. *Atmos. Chem. Phys.* **2016**, *16*, 1761–1771.
- (126) Tong, H.; Lakey, P.; Arangio, A.; Socorro, J.; Kampf, C. J.; Berkemeier, T.; Brune, W. H.; Poschl, U.; Shiraiwa, M. *Faraday Discuss.* **2017**, *200*, 251–270.
- (127) Browne, E. C.; Franklin, J. P.; Canagaratna, M. R.; Massoli, P.; Kirchstetter, T. W.; Worsnop, D. R.; Wilson, K. R.; Kroll, J. H. *J. Phys. Chem. A* **2015**, *119*, 1154–1163.
- (128) Lim, C. Y.; Browne, E. C.; Sugrue, R. A.; Kroll, J. H. *Geophys. Res. Lett.* **2017**, *44*, 2949–2957.
- (129) Cheng, C. T.; Chan, M. N.; Wilson, K. R. *J. Phys. Chem. A* **2016**, *120*, 5887–5896.
- (130) Cheng, C. T.; Chan, M. N.; Wilson, K. R. *Phys. Chem. Chem. Phys.* **2015**, *17*, 25309–25321.
- (131) Kroll, J. H.; Lim, C. Y.; Kessler, S. H.; Wilson, K. R. *J. Phys. Chem. A* **2015**, *119*, 10767–10783.
- (132) Kourtchev, I.; Doussin, J. F.; Giorio, C.; Mahon, B.; Wilson, E. M.; Maurin, N.; Pangui, E.; Venables, D. S.; Wenger, J. C.; Kalberer, M. *Atmos. Chem. Phys.* **2015**, *15*, 5683–5695.

- (133) Hinks, M. L.; Brady, M. V.; Lignell, H.; Song, M.; Grayson, J. W.; Bertram, A. K.; Lin, P.; Laskin, A.; Laskin, J.; Nizkorodov, S. A. *Phys. Chem. Chem. Phys.* **2016**, *18*, 8785–8793.
- (134) Li, Y.; Poeschl, U.; Shiraiwa, M. *Atmos. Chem. Phys.* **2016**, *16*, 3327–3344.
- (135) Lin, P.; Aiona, P. K.; Li, Y.; Shiraiwa, M.; Laskin, J.; Nizkorodov, S. A.; Laskin, A. *Environ. Sci. Technol.* **2016**, *50*, 11815–11824.
- (136) Bell, D. M.; Imre, D.; Martin, S. T.; Zelenyuk, A. *Phys. Chem. Chem. Phys.* **2017**, *19*, 6497–6507.
- (137) Chim, M. M.; Chow, C. Y.; Davies, J. F.; Chan, M. N. J. *Phys. Chem. A* **2017**, *121*, 1666–1674.
- (138) Davies, J. F.; Wilson, K. R. *Chem. Sci.* **2015**, *6*, 7020–7027.
- (139) Bannan, T. J.; Booth, A. M.; Jones, B. T.; O'Meara, S.; Barley, M. H.; Riipinen, I.; Percival, C. J.; Topping, D. *Environ. Sci. Technol.* **2017**, *51*, 3922–3928.
- (140) Huisman, A. J.; Krieger, U. K.; Zuend, A.; Marcolli, C.; Peter, T. *Atmos. Chem. Phys.* **2013**, *13*, 6647–6662.
- (141) Topping, D.; Riipinen, I.; Percival, C.; Bannan, T. *Environ. Sci. Technol.* **2017**, *51*, 7744–7745.
- (142) Wania, F.; Awonaike, B.; Goss, K. U. *Environ. Sci. Technol.* **2017**, *51*, 7742–7743.
- (143) Andreae, M. O.; Gelencser, A. *Atmos. Chem. Phys.* **2006**, *6*, 3131–3148.
- (144) Weggler, B. A.; Ly-Verdu, S.; Jennerwein, M.; Sippula, O.; Reda, A. A.; Orasche, J.; Groger, T.; Jokiniemi, J.; Zimmermann, R. *Environ. Sci. Technol.* **2016**, *50*, 10073–10081.
- (145) Lin, P.; Bluvshstein, N.; Rudich, Y.; Nizkorodov, S.; Laskin, J.; Laskin, A. *Environ. Sci. Technol.* **2017**, *51*, 11561.
- (146) Bluvshstein, N.; Lin, P.; Flores, J. M.; Segev, L.; Mazar, Y.; Tas, E.; Snider, G.; Weagle, C.; Brown, S. S.; Laskin, A.; Rudich, Y. *J. Geophys. Res. Atmos.* **2017**, *122*, 5441–5456.
- (147) Budisulistiorini, S. H.; Riva, M.; Williams, M.; Chen, J.; Itoh, M.; Surratt, J. D.; Kuwata, M. *Environ. Sci. Technol.* **2017**, *51*, 4415–4423.
- (148) Teich, M.; van Pinxteren, D.; Wang, M.; Kecorius, S.; Wang, Z. B.; Müller, T.; Mocnik, G.; Herrmann, H. *Atmos. Chem. Phys.* **2017**, *17*, 1653–1672.
- (149) Costabile, F.; Gilardoni, S.; Barnaba, F.; Di Ianni, A.; Di Liberto, L.; Dionisi, D.; Manigrasso, M.; Paglione, M.; Poluzzi, V.; Rinaldi, M.; Facchini, M. C.; Gobbi, G. P. *Atmos. Chem. Phys.* **2017**, *17*, 313–326.
- (150) Saleh, R.; Robinson, E. S.; Tkacik, D. S.; Ahern, A. T.; Liu, S.; Aiken, A. C.; Sullivan, R. C.; Presto, A. A.; Dubey, M. K.; Yokelson, R. J.; Donahue, N. M.; Robinson, A. L. *Nat. Geosci.* **2014**, *7*, 647–650.
- (151) Chen, Q. C.; Ikemori, F.; Mochida, M. *Environ. Sci. Technol.* **2016**, *50*, 10859–10868.
- (152) Chen, Q. C.; Miyazaki, Y.; Kawamura, K.; Matsumoto, K.; Coburn, S.; Volkamer, R.; Iwamoto, Y.; Kagami, S.; Deng, Y. G.; Ogawa, S.; Ramasamy, S.; Kato, S.; Ida, A.; Kajii, Y.; Mochida, M. *Environ. Sci. Technol.* **2016**, *50*, 10351–10360.
- (153) Aiona, P. K.; Lee, H. J.; Leslie, R.; Lin, P.; Laskin, A.; Laskin, J.; Nizkorodov, S. A. *ACS Earth and Space Chemistry* **2017**, *1*, 522–532.
- (154) Kampf, C. J.; Filippi, A.; Zuth, C.; Hoffmann, T.; Opatz, T. *Phys. Chem. Chem. Phys.* **2016**, *18*, 18353–18364.
- (155) Aiona, P. K.; Lee, H. J.; Lin, P.; Heller, F.; Laskin, A.; Laskin, J.; Nizkorodov, S. A. *Environ. Sci. Technol.* **2017**, *51*, 11048.
- (156) Lin, P.; Liu, J.; Shilling, J. E.; Kathmann, S. M.; Laskin, J.; Laskin, A. *Phys. Chem. Chem. Phys.* **2015**, *17*, 23312–23325.
- (157) Zhang, X.; Barraza, K. M.; Upton, K. T.; Beauchamp, J. L. *Chem. Phys. Lett.* **2017**, *683*, 76–82.
- (158) Enami, S.; Vecitis, C. D.; Cheng, J.; Hoffmann, M. R.; Colussi, A. J. *J. Phys. Chem. A* **2007**, *111*, 13032–13037.
- (159) Enami, S.; Hoffmann, M. R.; Colussi, A. J. *J. Phys. Chem. A* **2014**, *118*, 4130–4137.
- (160) Enami, S.; Colussi, A. J. *J. Phys. Chem. Lett.* **2017**, *8*, 1615–1623.
- (161) Enami, S.; Colussi, A. J. *Phys. Chem. Chem. Phys.* **2017**, *19*, 17044–17051.
- (162) Enami, S.; Colussi, A. J. *J. Phys. Chem. A* **2017**, *121*, 5175–5182.
- (163) Enami, S.; Hoffmann, M. R.; Colussi, A. J. *J. Phys. Chem. Lett.* **2017**, *8*, 3888–3894.
- (164) Ciuraru, R.; Fine, L.; Pinxteren, M. v.; D'Anna, B.; Herrmann, H.; George, C. *Environ. Sci. Technol.* **2015**, *49*, 13199–13205.
- (165) Chiu, R.; Tinel, L.; Gonzalez, L.; Ciuraru, R.; Bernard, F.; George, C.; Volkamer, R. *Geophys. Res. Lett.* **2017**, *44*, 1079–1087.
- (166) Bernard, F.; Ciuraru, R.; Boréave, A.; George, C. *Environ. Sci. Technol.* **2016**, *50*, 8678–8686.
- (167) Bruggemann, M.; Hayeck, N.; Bonnineau, C.; Pesce, S.; Alpert, P. A.; Perrier, S.; Zuth, C.; Hoffmann, T.; Chen, J.; George, C. *Faraday Discuss.* **2017**, *200*, 59–74.
- (168) Rapf, R. J.; Perkins, R. J.; Yang, H.; Miyake, G. M.; Carpenter, B. K.; Vaida, V. J. *Am. Chem. Soc.* **2017**, *139*, 6946–6959.
- (169) Rossignol, S.; Tinel, L.; Bianco, A.; Passananti, M.; Brigante, M.; Donaldson, D. J.; George, C. *Science* **2016**, *353*, 699–702.
- (170) Sui, X.; Zhou, Y.; Zhang, F.; Chen, J.; Zhu, Z.; Yu, X.-Y. *Phys. Chem. Chem. Phys.* **2017**, *19*, 20357–20366.
- (171) Cochran, R. E.; Laskina, O.; Trueblood, J. V.; Estillore, A. D.; Morris, H. S.; Jayarathne, T.; Sultana, C. M.; Lee, C.; Lin, P.; Laskin, J.; Laskin, A.; Dowling, J. A.; Qin, Z.; Cappa, C. D.; Bertram, T. H.; Tivanski, A. V.; Stone, E. A.; Prather, K. A.; Grassian, V. H. *Chem.* **2017**, *2*, 655–667.
- (172) Cochran, R. E.; Ryder, O. S.; Grassian, V. H.; Prather, K. A. *Acc. Chem. Res.* **2017**, *50*, 599–604.
- (173) Quinn, P. K.; Collins, D. B.; Grassian, V. H.; Prather, K. A.; Bates, T. S. *Chem. Rev.* **2015**, *115*, 4383–4399.
- (174) Sultana, C. M.; Collins, D. B.; Prather, K. A. *Environ. Sci. Technol.* **2017**, *51*, 3660–3668.
- (175) Cahill, J. F.; Darlington, T. K.; Fitzgerald, C.; Schoepp, N. G.; Beld, J.; Burkart, M. D.; Prather, K. A. *Anal. Chem.* **2015**, *87*, 8039–8046.
- (176) Cochran, R. E.; Laskina, O.; Jayarathne, T.; Laskin, A.; Laskin, J.; Lin, P.; Sultana, C.; Lee, C.; Moore, K. A.; Cappa, C. D.; Bertram, T. H.; Prather, K. A.; Grassian, V. H.; Stone, E. A. *Environ. Sci. Technol.* **2016**, *50*, 2477–2486.
- (177) Forestieri, S. D.; Cornwell, G. C.; Helgestad, T. M.; Moore, K. A.; Lee, C.; Novak, G. A.; Sultana, C. M.; Wang, X. F.; Bertram, T. H.; Prather, K. A.; Cappa, C. D. *Atmos. Chem. Phys.* **2016**, *16*, 9003–9018.
- (178) Sultana, C. M.; Al-Mashat, H.; Prather, K. A. *Anal. Chem.* **2017**, *89*, 10162–10170.
- (179) Gunsch, M. J.; Kirpes, R. M.; Kolesar, K. R.; Barrett, T. E.; China, S.; Sheesley, R. J.; Laskin, A.; Wiedensohler, A.; Tuch, T.; Pratt, K. A. *Atmos. Chem. Phys.* **2017**, *17*, 10879–10892.